ADVANCED SCIENCE Open Access
www.advancedscience.com

# Gene Electrotransfer via Conductivity-Clamped Electric Field Focusing Pivots Sensori-Motor DNA Therapeutics: "A Spoonful of Sugar Helps the Medicine Go Down"

*Jeremy L. Pinyon, Georg von Jonquieres, Edward N. Crawford, Amr Al Abed, John M. Power, Matthias Klugmann, Cherylea J. Browne, David M. Housley, Andrew K. Wise, James B. Fallon, Robert K. Shepherd, John Y. Lin, Catherine McMahon, David McAlpine, Catherine S. Birman, Waikong Lai, Ya Lang Enke, Paul M. Carter, James F. Patrick, Robert D. Gay, Corinne Marie, Daniel Scherman, Nigel H. Lovell, and Gary D. Housley**

**Viral vectors and lipofection-based gene therapies have dispersion-dependent transduction/transfection profiles that thwart precise targeting. The study describes the development of focused close-field gene electrotransfer (GET) technology, refining spatial control of gene expression. Integration of fluidics for precise delivery of "naked" plasmid deoxyribonucleic acid (DNA) in sucrose carrier within the focused electric field enables negative biasing of near-field conductivity ("conductivity-clamping"–CC), increasing the efficiency of plasma membrane molecular translocation. This enables titratable gene delivery with unprecedently low charge transfer. The clinic-ready bionics-derived CC-GET device achieved neurotrophin-encoding miniplasmid DNA delivery to the cochlea to promote auditory nerve regeneration; validated in deafened guinea pig and cat models, leading to improved central auditory tuning with bionics-based hearing. The performance of CC-GET is evaluated in the brain, an organ problematic for pulsed electric field-based plasmid DNA delivery, due to high required currents causing Joule-heating and damaging electroporation. Here CC-GET enables safe precision targeting of gene expression. In the guinea pig, reporter expression is enabled in physiologically critical brainstem regions, and in the striatum (globus pallidus region) delivery of a red-shifted channelrhodopsin and a genetically-encoded $Ca^{2+}$ sensor, achieved photoactivated neuromodulation relevant to the treatment of Parkinson's Disease and other focal brain disorders.**

## 1. Introduction

Delivery technologies are central to enabling deoxyribonucleic acid (DNA) and ribonucleic acid (RNA)-based therapeutics. "Pre-Covid," viral vectors were the most widely adopted vehicle,[1] while nanoparticle packaging now dominates RNA therapeutics and is increasingly being utilized in clinical trials.[2] These technologies are variously challenged by uncontrolled dispersion of the active agent, packaging limitations, stability, liver toxicity, immunoincompatibility (affecting present and future treatments), and cost.[3] Gene electrotransfer (GET) offers an alternative delivery strategy, where electric pulses cause naked polyanionic nucleic acid molecules (NAs) to bind to the cathode-facing plasma membranes of cells in target tissues.[4] This delivery is virtually instantaneous and modulated by electric field strength. The membrane-bound NAs undergo endocytosis, and in the case of DNA, a fraction is transported to the nucleus to support episomal gene transcription.[5] GET is

The ORCID identification number(s) for the author(s) of this article can be found under https://doi.org/10.1002/advs.202401392



**DOI: 10.1002/advs.202401392**

J. L. Pinyon, G. von Jonquieres, E. N. Crawford, A. A. Abed, J. M. Power, M. Klugmann, C. J. Browne, D. M. Housley, N. H. Lovell, G. D. Housley
Translational Neuroscience Facility
Department of Physiology
School of Biomedical Sciences
Graduate School of Biomedical Engineering
Tyree Institute for Health Engineering (IHealthE)
UNSW
Sydney, NSW 2052, Australia
E-mail: g.housley@unsw.edu.au

distinct from transient pore formation in the plasma membrane, termed "electroporation," which is generated by high voltage pulsed electric fields and enables translocation of low molecular weight molecules.[6,7] This is exemplified by the demonstration of progressive take-up of the impermeant fluorescent dye propidium iodide following delivery of the pulsed electric field (via transient and irreversible electroporation), while (fluorescently tagged) naked DNA binding to the plasma membrane is limited to the duration of the pulse train,[6] followed by slower internalization in association with clathrin and caveolin-/lipid raft – mediated endocytosis; validated by dose-dependent pharmacological inhibition of reporter gene expression.[5]

At present, clinical applications for GET are primarily focused on oncology, notably supporting the delivery of DNA vaccines driving immunotherapies, such as interleukin 12-encoding DNA to stimulate innate immune responses to melanoma using devices with multiple needle electrodes for "open-field" electrotransfer.[8] There are a range of medical devices being used in clinical trials for reversible and irreversible electroporation, GET, and electrochemotherapy applications.[3,9] The invasiveness of the electrode configurations for "open-field" GET, and the requirement for high voltages and currents to generate efficacious pulsed electric fields, cause tissue injury,[10] limiting the application scope, and are painful. However, "close-field" GET has been established by electric field focusing (local electric field compression) utilizing multi-channel linear electrode arrays (derived from cochlear implant technology), where the target tissue surrounding the GET probe is exposed to an orthogonal-compressed electric field, rather than the homogenous electric field exposure inherent to having the target tissue between two or more electrodes.[11–15]

Here we describe the enablement of enhanced close-field GET which incorporates clamping of conductivity within the focused electric field, using a sucrose carrier for the negatively charged plasmid DNA. This enhances the electric field focusing and minimizes charge transfer to achieve suprathreshold electric field strength. The efficacy and safety of this conductivity-clamped gene electrotransfer (CC-GET) technology were evaluated in guinea pig and cat cochlea models supporting the development of a clinical CC-GET gene delivery device and neurotrophin-encoding therapeutic miniplasmid DNA, for application in regenerative medicine to regrow the atrophied auditory nerve in patients receiving a cochlear implant (CI), closing the "neural gap" to enhance the "bionic ear" neural interface. The utility of CC-GET was further validated in the brain, a tissue particularly vulnerable to the high voltage/current profiles utilized for conventional GET. Studies here demonstrate that CC-GET in the guinea pig brain enables the safe targeted expression of reporter and optogenetic gene cassettes at charge transfer levels which would be ineffective using conventional GET. The development of CC-GET establishes a pathway for complementary gene therapy to augment cochlear and brain bionics and more broadly to achieve spatially controlled titratable DNA electrotransfer for sensorimotor disorders, and other deep-tissue pathophysiological targets throughout the body.

## 2. Results and Discussion

### 2.1. Localized Conductivity-Clamping Enhances Array-Based Electric Field Compression for DNA Electrotransfer

The CC-GET device utilizes a linear electrode array to create an "electro-lens" that compresses the electric field orthogonally, for optimal plasmid DNA electrotransfer efficiency, where the electric field strength ($V_f$/cm) is the driver for the molecular translocation of DNA to the cell.[12] Complementing this electric field shaping, a linear electrode array lends itself to the use of low-conductance DNA carrier solution in the immediate proximity to the electrodes ("conductivity-clamping") to enhance the

J. L. Pinyon
Charles Perkins Centre
School of Medical Sciences
Faculty of Medicine and Health
University of Sydney
Sydney, NSW 2006, Australia
C. J. Browne
Medical Sciences
School of Science
Western Sydney University
Sydney, NSW 2560, Australia
A. K. Wise, J. B. Fallon, R. K. Shepherd
Bionics Institute
384–388 Albert Street, East Melbourne, VIC 3002, Australia
A. K. Wise, J. B. Fallon, R. K. Shepherd
Medical Bionics
Department of Otolaryngology
University of Melbourne
Melbourne, VIC 3002, Australia
J. Y. Lin
Tasmanian School of Medicine
University of Tasmania
Hobart, TAS 7001, Australia
C. McMahon, D. McAlpine, C. S. Birman
Faculty of Medicine and Health Sciences
The Hearing Hub
Macquarie University
Sydney 2109, Australia
C. S. Birman
Faculty of Medicine and Health
University of Sydney
Sydney, NSW 2006, Australia
C. S. Birman
Department of Otolaryngology
Royal Prince Alfred Hospital
Camperdown, NSW 2050, Australia
C. S. Birman, W. Lai
NextSense
Royal Institute of Deaf and Blind Children
Gladesville, NSW 2111, Australia
Y. L. Enke, P. M. Carter, J. F. Patrick, R. D. Gay
Cochlear Limited
Macquarie University
University Avenue, Macquarie Park, NSW 2109, Australia
C. Marie, D. Scherman
CNRS, Inserm, UTCBS
Université Paris Cité
Paris F-75006, France
C. Marie
Chimie ParisTech
Université PSL
Paris 75005, France
D. Scherman
Fondation Maladies Rares
96 rue Didot, Paris 75014, France

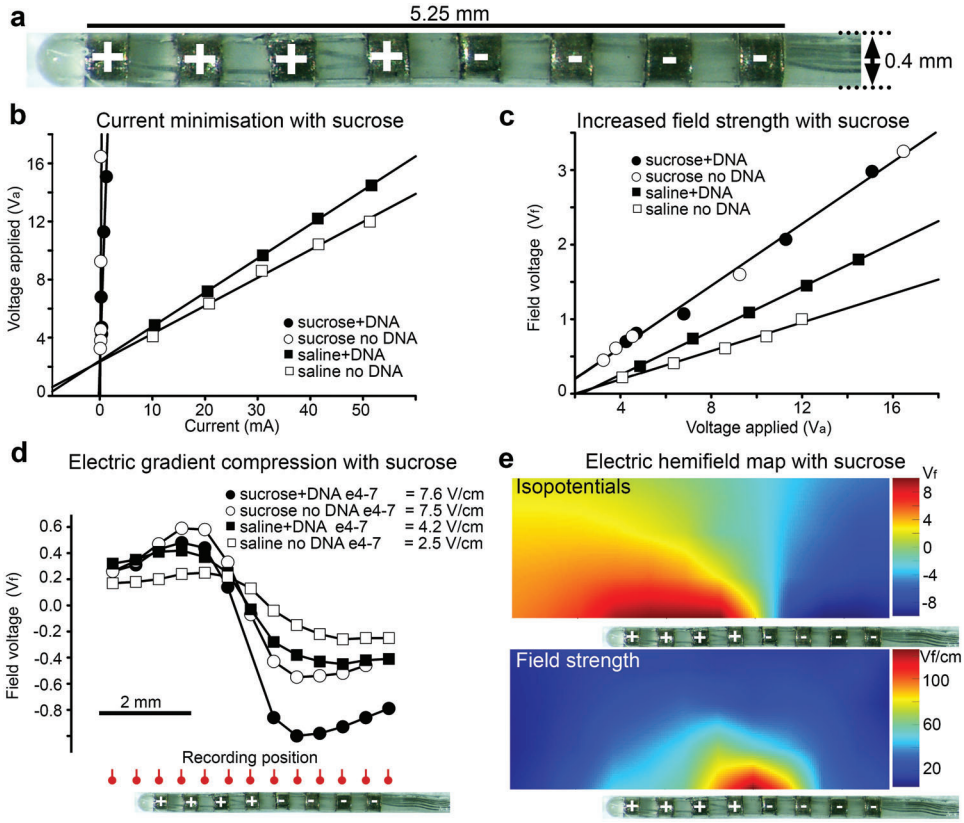


**Figure 1.** Nonconductive sucrose carrier amplifies bionic array electric field strength. a) Image of an 8-electrode GET array (derived from a preclinical cochlear implant). b) Constant current pulses of increasing amplitude across the ganged electrodes in normal saline, or the nonconducting 10% sucrose carrier, with or without DNA (2 μg $\mu L^{-1}$) generate applied voltages ($V_a$) on the electrodes. Note the amplification of $V_a$ provided by "conductivity-clamping" using a sucrose carrier. c) Sucrose-enhanced field voltage ($V_f$) measured at a reference point 0.5 mm lateral to electrode 7 (second from left in (A)), compared with saline carrier. d) $V_f$ sampled along the array demonstrates the electric "lensing" effect, with the greatest change in voltage/slope around the null point in the middle of the array. DNA + sucrose ~ doubled the electric field strength ($\Delta V_f/\Delta d$) between electrodes 4–7 compared with saline + DNA. e) Isopotential map (hemifield) and derived electric field map for sucrose carrier (40 V applied, 100 ms pulses). Data from B to E are reflected in the US patent.[16] Data for 0.9% NaCl without DNA in (D) is ref. [14]. See also Supporting Information primary figure commentary.

electric field strength and hence electrophoretic delivery of DNA to the plasma membrane. The clamping of extracellular conductivity using isotonic sucrose carrier with negatively charged DNA as the major charge species was evaluated to determine the effect on the voltage in close-field (**Figure 1**).

The relationship between constant current pulse amplitude and the applied voltage ($V_a$) at the GET array (Figure 1a) (delivered by an analog-controlled Digitimer DS5 stimulator in voltage mode) was compared between use of 2 μg $\mu L^{-1}$ DNA (salmon sperm sheared DNA) in isotonic sucrose (10%) and normal saline (0.9% NaCl) + DNA (Figure 1b). The sucrose carrier increased resistivity across the array by ≈43-fold (sucrose + DNA = 12.08 kΩ; 0.9% saline + DNA 0.28 kΩ). Thus, by way of example, ≈14.5 V applied voltage ($V_a$) would elicit a 1.2 mA current pulse in sucrose + DNA, whereas this $V_a$ would cause a 51.6 mA current pulse in saline + DNA. By comparison, in the absence of DNA, the array resistance in sucrose was 78.38 kΩ, compared with 0.23 kΩ for saline only; thus DNA was the principal charge species in sucrose (650% increase in conductivity), compared with saline (20% change). Further, the sucrose carrier provided an added advantage with respect to electric field strength, where the voltage in the field ($V_f$) measured adjacent to the electrode array was 42% greater compared with using saline at equivalent $V_a$ (Figure 1c). Measured 0.5 mm orthogonal to electrode 7 (anode # 3), sucrose + DNA = 0.209 $V_f/V_a$ compared to 0.147 $V_f/V_a$ for saline + DNA; reflecting the differential conductivity. In summary, the substitution of sucrose + DNA as a carrier over conventional saline + DNA provides ≈75× increased benefit in effective voltage achieved in the field for equivalent current delivery. Given that joule heating of tissue is dependent on current squared multiplied by resistance, minimization of current using sucrose carrier represents a significant advantage.

Extending from these reference point measurements, the change in $V_f$ adjacent to all eight electrodes in the array was measured using 100 ms × 5 V pulses; sampling at 0.5 mm steps, 0.5 mm lateral to the array (Figure 1d). This demonstrated that adding DNA to the saline carrier increased the maximum electric field strength (slope) by 68% (4.2 V $cm^{-1}$ compared with 2.5 V $cm^{-1}$, as peak slope about the null point between the four ganged anodes and four ganged cathodes, sampled at ≈95 ms). In comparison, the use of sucrose carrier + DNA at the same applied voltage (5 V), further increased the field strength (7.6 V $cm^{-1}$) by 81% above the saline + DNA level. Electric field mapping was then undertaken adjacent to the electrode array using a

 

translational stage at 0.5 mm resolution steps, with 10% sucrose carrier, using 100 ms × 40 V pulses, which is the suprathreshold for DNA electrotransfer[12] (Figure 1e). This demonstrated the spherical electric field lensing effect of the DNA electrotransfer array in the sucrose carrier.

### 2.2. Validation of High Efficiency Gene Expression Using CC-GET

Given the evident improvement in electric field strength achieved by local clamping of conductivity using a 10% sucrose carrier, CC-GET was functionally validated in a human embryonic kidney 293 (HEK293) cell monolayer model (after ref. [12]). These experiments showed that sustained exposure of these cells to 10% sucrose + CMVp-hrGFPnls plasmid DNA (2 μg μL$^{-1}$; Figure S1A, Supporting Information) was innocuous and demonstrated significantly improved gene expression over the use of a conventional saline-based carrier. This was demonstrated though the increased surface area of the circular field of green fluorescent protein (GFP)+ve transfected cells centered on the null point of the DNA delivery probe between the ganged anodes and cathodes (sucrose carrier = 21.7 ± 2.8 mm$^2$ GFP+ve cells, $n$ = 5; saline = 13.5 ± 1.3 mm$^2$ GFP+ve cells, $n$ = 9; $p$ = 0.0103, Student's $t$-test; 3 × 100 ms × 35 V pulses; Figure S2A, Supporting Information). This represented a 27% expansion in the diameter of the field of transfected HEK293 cells for the same fixed $V_a$; where the perimeter reflects the boundary electric field threshold for gene electrotransfer (e.g., ≈2.5 mm distal to the array centroid in the case of 10% sucrose carrier). This GFP reporter study, with 3 days in cell culture, validated the field-strength gain attributable to local conductivity-clamping, at a fixed voltage, determined in the biophysical measurements shown in Figure 1c,d. This model was then extended to quantify the efficiency of GET within the field of GFP-positive cells using the same pulse parameters and reporter plasmid, comparing saline versus sucrose carriers. The cells were fixed after 24 h (to limit cell division[17]) and the nuclei were labeled with DAPI (4'-6'-diamino-2-phenylindole). A prescribed region of interest (ROI) within the field of GFP-expressing cells was imaged to provide counts for GFP-positive cells and GFP-negative – DAPI-only cells. These data (Figure S2A–C, Supporting Information) replicated the original finding of increased area of GFP cell expression with sucrose carrier (sucrose = 14.25 ± 0.98 mm$^2$; saline = 6.97 ± 1.17 mm$^2$; $n$ = 6 per group; $p$ = 0.000733, $t$-test). Two-way ANOVA of the cell count data for GFP positive cells and DAPI positive (GFP negative) cells showed a significant impact of GET on cell survival using a saline carrier (sucrose GFP = 141.83 ± 34.90 cells; saline GFP = 73.83 ± 11.43 cells; sucrose DAPI = 538.00 ± 112.18 cells; saline DAPI = 286.67 ± 57.66 cells; $n$ = 6 per group; $p$ = 0.0175 Holm-Sidak post hoc comparison), (Figure S2B–D, Supporting Information). While cell density was reduced with saline-based GET, relative gene expression efficiency within the ROIs (% GFP positive cells / total cell number) was equivalent for both sucrose and saline carriers (sucrose = 20.349 ± 1.056% efficiency; saline = 21.792 ± 2.812% efficiency; $p$ = 0.641, $t$-test; Figure 2d).

The evident impact of saline carrier on cell density was investigated using an experimental design where, 1 h after GET using either sucrose or saline carriers, the cell impermeant fluorescent marker propidium iodide (PI) was added to the culture media for 5 min, to label cells with irreversible permeabilization, followed by fixation and imaging. Conductivity – clamping provided by the sucrose carrier was determined from local resistance measurements, showing a 92% average reduction in current for the 35 V pulses (sucrose = 2.76 ± 0.03 mA; saline = 35.58 ± 1.98 mA; $p$ < 0.001 $t$-test). This study demonstrated a significant injury margin for the saline carrier, proximal to where the GET electrode array had been positioned over the cell monolayer; consistent with known irreversible electroporation arising from high current flux.[18] The PI signal was minimal for the sucrose carrier, where the measured margin largely represented mechanical injury from electrode placement. Average PI areas: saline = 10.23 ± 1.62 mm$^2$ ($n$ = 6); sucrose = 2.58 ± 0.47 mm$^2$ ($n$ = 5); $p$ = 0.00245 $t$-test, (Figure S2E–G, Supporting Information).

Having identified the advantage of CC-GET, we sought to establish the minimum (and hence safest) charge delivery protocol for effective gene expression. Experiments were performed using CMVp-hrGFPnls plasmid (2 μg μL$^{-1}$) with HEK293 cell monolayers, varying current amplitude applied to the clinical CC-GET DNA delivery probe with 3 × 100 μs square wave pulses (Figure S3, Supporting Information). This demonstrated a threshold of ≈5 mA (Figure S3B, Supporting Information) ($p$ = 0.00017, single sample $t$-test), with a field of GFP+ve cells of 0.77 ± 0.08 mm$^2$ ($n$ = 6), with a nonlinear increase to 12.3 ± 1.9 mm$^2$ ($n$ = 5) using 15 mA pulses ($p$ = 0.002, one way ANOVA on ranks) (Figure S3D, Supporting Information).

The scalability of the electric field created by the linear DNA electrotransfer array was determined by simplification of the array from a multi-node "tandem" electrode configuration to a device that comprised two discrete elongated current donors and receiver Pt/Ir electrode surfaces (2 mm length, 400 μm diameter), where systematic changes in the dispersion of the electric field "lens" was achieved by separation of these two electrodes on a silicone core backbone. These experiments showed that the "lensing" for focused electric field GET was controllable by adjusting the separation between the electrode poles (**Figure 2a–h**). For a fixed charge transfer, the surface area of transduced HEK293 cells expressing the GFP reporter varied around fourfold, from (7.13 ± 1.34 to 31.08 ± 3.24 mm$^2$), with lens separation of 0.2–4.0 mm respectively; representing a decompression of the electric field (Figure 2g). In conjunction with the Monte Carlo simulation of the electric fields (Figure 2h), the perimeters of GFP+ve transfected HEK293 cells established the electric field boundary condition for DNA electrotransfer at $V_f$/d = 120.8 ± 20.2 V cm$^{-1}$ (mean ± SD). These experiments utilized 30 mA constant current (100 μs) delivered in a 9% sucrose + 0.09% NaCl solution (modeling physiologically relevant conductivity-clamping) via 120 V applied driving voltage. These findings highlight the capability of CC-GET to achieve "dial-up" spatial control of gene expression with minimal charge transfer.

The scala tympani fluid compartment of the human cochlea that receives the CI varies in diameter from ≈2.5 mm at the base to ≈0.75 mm at the upper insertion position for a CI array (25 mm in length).[19] These experiments confirmed that the ganged four-electrode configuration for the anode and cathode elements of the GET array, with a 350 μm separation between the anode and cathode gangs, as previously used in initial proof of concept studies,[11,12,14,15,17] provided an ideal electric field shape to achieve the targeted delivery of naked DNA encoding

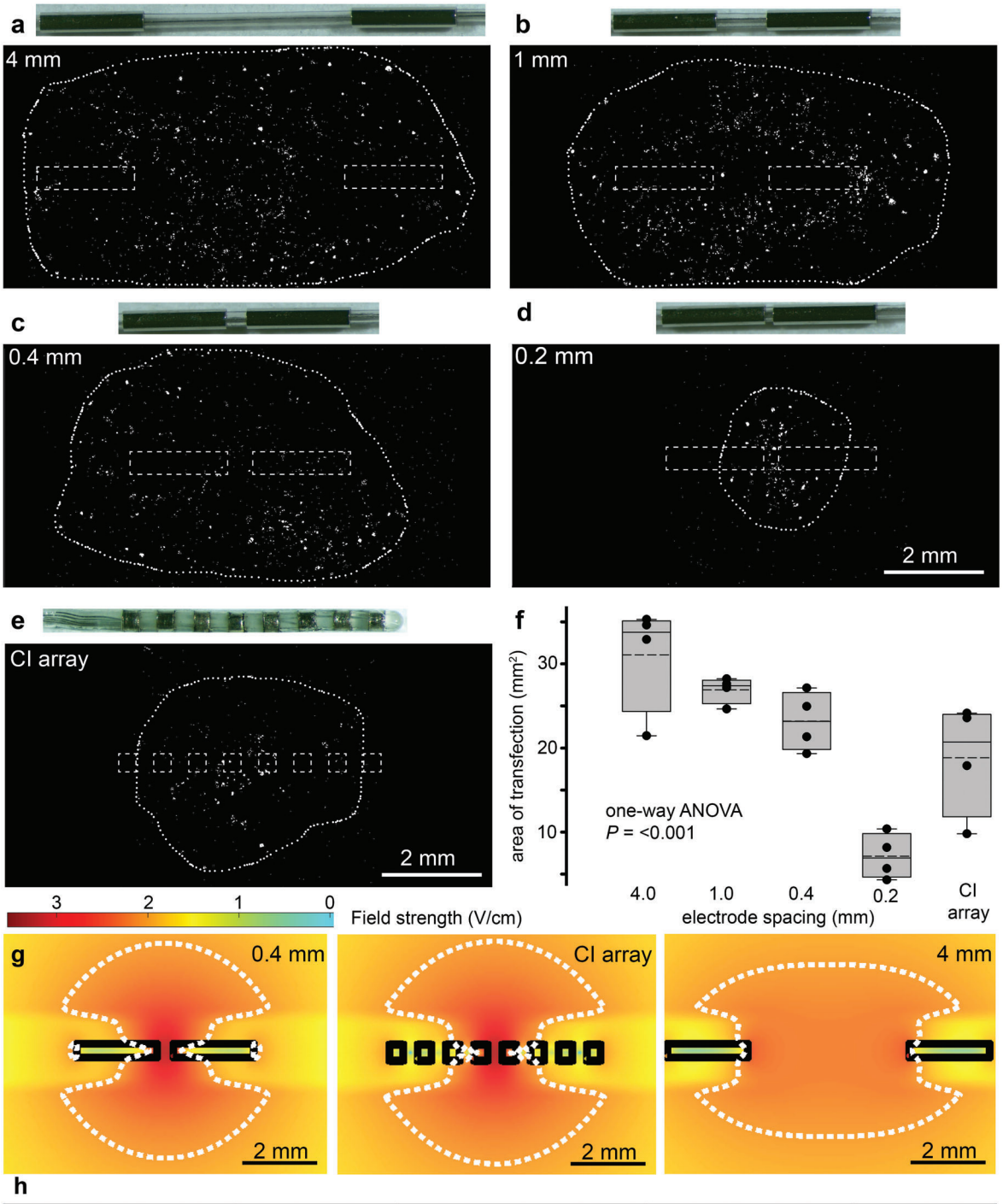


h

| CC-GET 'Lens' separation (mm) | Resistance (Ω) | Experiment area mean ± sem ($mm^2$) | Model area ($mm^2$) | Threshold (V/cm) |
|---|---|---|---|---|
| 0.2 | 3339 | 7.13 ± 1.34 | 17.30 | 120.8 |
| 0.4 | 4398 | 23.20 ± 1.75 | 17.65 | 120.8 |
| 1.0 | 6824 | 26.91 ± 0.79 | 18.67 | 120.8 |
| 4.0 | 15360 | 31.08 ± 3.24 | 21.46 | 120.8 |
| 8-electrode CI (0.35) | 3811 | 18.85 ± 3.33 | 18.90 | 120.8 |

**Figure 2.** Electric field "lensing" via the CC-GET array enables spatial focusing of gene expression. a–d) Variation in the separation between the extended conductive surfaces of the linear CC-GET array (modeling the ganged discrete electrode elements as shown in (e), acts as a "lens" to change the spread

neurotrophins to the scala tympani mesenchymal cells immediately adjacent to a subsequently inserted (permanent) CI array. The bionic arrays used for chronic deep brain stimulation (DBS) to manage Parkinson's Disease dyskinesia utilize a similar electrode array configuration and pulse parameters[20] and hence the tuning of the CC-GET array was predicted to enable safe and effective DNA delivery to the brain.

### 2.3. Development of a Clinical CC-GET Medical Device for Auditory Nerve Regeneration to Augment Bionic Ear Functionality

Development of the clinical CC-GET device was achieved by biomedical engineers at Cochlear Ltd by reengineering a conventional 22 half-band Pt/Ir CI array (Cochlear Nucleus CI622 array derivative; Cochlear Ltd) to produce the 2 × 4 ganged electrodes at 0.4 mm "lens" spacing as above (electrodes e15–e22), with the addition of a second pair of ganged electrodes (e7–e14). This arrangement enables more basal targeting of DNA electrotransfer by switching between array elements and delivering a second pulse train (**Figure 3**). To achieve localized conductivity-clamping, the microfluidic delivery capability was integrated into the CC-GET array by molding a lumen into the silicone, beneath the half-banded electrodes, enabling local displacement of the cochlear perilymph solution with the therapeutic DNA in 10% sucrose carrier. Given that the scala tympani compartment is effectively blind-ended, DNA delivery from the tip of the inserted array results in DNA solution displacing cochlear perilymph around the CC-GET device (Figure 3b), clamping the electric field as modeled. The efficacy of the switching between successive electrode elements within the cochlear CC-GET device to achieve DNA electrotransfer along the length of the perilymphatic compartment was modeled in vitro (Figure 3e). Nuclear localized GFP fluorescence of HEK293 cells showed titratable "painting" of DNA electrotransfer over an extending distance when a pulse train (3 × 100 ms) was delivered to the apical-most ganged electrode set (e15–e22) and then the more basal set (e7–e14) (1–3 mA range), modeling electrotransfer to the mesenchymal cells of the cochlea scala tympani immediately adjacent to the CC-GET device.

### 2.4. CC-GET Targeting Guinea Pig Cochlear Perilymphatic Mesenchymal Cells In Vivo

A 4-month in vivo safety and efficacy study was conducted to validate CC-GET for targeted gene expression in the mesenchymal cells of the guinea pig cochlea scala tympani compartment. These cells are the target for neurotrophin gene augmentation, as they are closest to the CI array, and their secretion of the recombinant neurotrophins establishes a gradient for directed regeneration of the atrophied spiral ganglion afferent fibers, closing the neural gap with the CI array (after ref. [11]). These experiments were undertaken in normal hearing guinea pigs using an enhanced GFP (eGFP) reporter sequence incorporated into the pFAR4 miniplasmid backbone (**p**lasmid **F**ree of **A**ntibiotic **R**esistance; after ref. [21]). The pFAR4 plasmid is compliant with the European Medicines Agency guidelines limiting the use of plasmids which could result in misdirected electrotransfer of antibiotic resistance genes to commensal bacteria.[22] The experiments used the clinical CC-GET device with an optimized pulse train (10 × 100 µs capped at 50 mA). The custom control system developed for the clinical application captured the current and voltage parameters for each current pulse delivered, which enabled measurement of the local resistance via the CC-GET array. The geometry of the guinea pig cochlea constrained the electrotransfer to the basal turn region, which was targeted using the apical eight-ganged electrodes of the clinical CC-GET device (zone 1 of Figure 3d). The DNA electrotransfer of the pFAR4-CMVp-eGFP miniplasmid (Figure S1B, Supporting Information) was performed under isoflurane anesthesia by insertion of the CC-GET array into the cochlear scala tympani via a perforation in the round window membrane. Fifty microliters of the DNA solution (2 µg µL$^{-1}$ pFAR4-CMVp-eGFP DNA in 10% sucrose; 0.5 mM NaOH (added to achieve physiological pH)) was delivered at 10 µL min$^{-1}$. The displacement of cochlear perilymph and enhancement of the electrotransfer biophysical profile achieved by conductivity-clamping via sucrose carrier infusion into scala tympani was confirmed by comparison of resistance just prior to commencing DNA infusion (mean = 770 ± 60 Ω) with the increased resistance at the time of electrotransfer (mean = 3.78 ± 0.56 kΩ; $n = 3$; $p = 0.0391$, paired $t$-test, $n = 3$; Table S1, Supporting Information). Across 12 experiments, the applied voltage required to achieve the constant current pulses ranged from 70 to 120 V ($V_a$ mean = 103.4 ± 5.51 V), where the upper limit reflected the compliance limit of the constant current stimulator (120 V; current pulse range 29–50 mA; mean = 45.1 ± 1.98 mA) dictated by the local resistance achieved by infusion of the sucrose carrier (2.40 ± 0.24 kΩ) (Table S1, Supporting Information). The resulting expression of the eGFP reporter was determined by hemisectioning decalcified cochleae and acquiring confocal images that captured the mesenchymal cell surface lining the perilymphatic scalae. Figure S4 (Supporting Information) shows the pronounced eGFP reporter fluorescence 4 days post CC-GET, with a significant drop-off by 2 weeks, and minimal cells expressing GFP at 16 weeks ($p = 0.031$, ranked ANOVA). These data are consistent with the turnover of the cochlear mesenchymal cells as previously described.[17] Here, using CC-GET, reliable GFP expression was achieved using 45 µC charge transfer, which is close to a thousand-fold improvement over the ≈40 mC minimum effective charge delivery previously required for close-field GET to cochlear mesenchymal cells without conductivity-clamping.[11]

of the electric field for the same charge transfer, where the CMVp-hrGFPnls plasmid DNA in 9% sucrose (0.09% NaCl) was delivered to HEK293 cell monolayers (10 × 100 µs, 400 µs interpulse interval, 30 mA square wave pulses; requiring 120 V applied; ≈30 µC total charge transfer; ≈4 kΩ local resistance). f) Boxplots of areas of transfected cells relative to electrode separation show 25% and 75% boundaries, with 95% limits as bars; lines indicate median, dashed lines indicate means, data overlaid ($n = 4$ per group). g) Monte Carlo modeling of electric fields across the configurations. The dashed perimeter, established by comparison with the perimeter of the fields of the bioreporter transfected HEK293 cells reflects the electric field threshold for DNA electrotransfer (120.8 V cm$^{-1}$). h) The predicted electric field threshold was validated in silico by further simulations using the clinical CC-GET device. See also Supporting Information – methods and primary figure commentary.

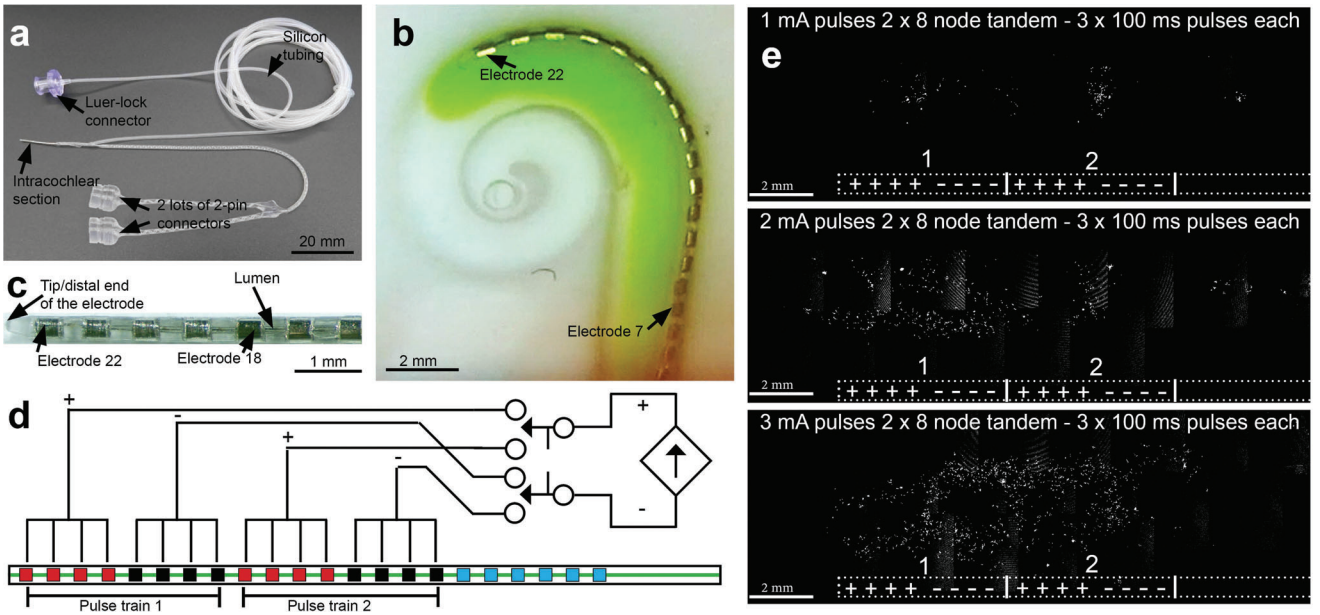


**Figure 3.** Design of the clinical CC-GET linear array for scalable targeting of plasmid DNA delivery to the cochlea. a) Intracochlear array of 22 half-band Pt/Ir electrodes incorporates a lumen that delivers the DNA in sucrose carrier solution via the tip (provided by Cochlear Ltd.). b) Image from a modeled human cochlea scala tympani fluid compartment, showing insertion of the CC-GET array, with green dye demonstrating how, in clinical application, the DNA in sucrose carrier solution would displace the perilymph and clamp the conductivity around the array, resulting in amplification of the electric field produced by the constant current pulses. c) Detail of the tip of the clinical CC-GET array showing the electrode elements and the internal lumen. d) Diagram of array "zone" switching to enable successive DNA electrotransfer to adjacent zones (e22–e15; e14–e7). e) CMVp-hrGFPnls plasmid DNA electrotransfer to HEK293 cell monolayers with increasing current. Data from (E) are reflected in US patent ref. [16]. Modeling of the electric field generated for GET by this device within the guinea pig cochlea is described in ref. [13].

### 2.5. Auditory Nerve Regeneration in the Deafened Guinea Pig Cochlea Using a Therapeutic Humanized Dual Neurotrophin-Encoding Miniplasmid DNA

The efficacy of our candidate therapeutic neurotrophin miniplasmid DNA (pFAR4-CMVp-BDNF-IRES-NT3; Figure S1C, Supporting Information) for auditory nerve regeneration was evaluated in the deafened guinea pig model ($n$ = 4). This molecule includes a bicistronic expression cassette comprising codon-optimized human brain-derived neurotrophic factor (BDNF) and neurotrophin-3 (NT3) elements. Prior to the in vivo experiments, secretion of the recombinant BDNF and NT3 neurotrophins was validated in HEK293 cells via ELISA (**Figure 4**). These in vitro experiments included the use of trains of monophasic, or varying polarity, pulses to demonstrate a correlation between the expression of a cocktail of a CMVp-mCHERRYnls reporter plasmid (Figure S1D, Supporting Information) alongside the clinical neurotrophin miniplasmid pFAR4-CMVp-BNDF-IRES-NT3. These HEK293 cell-based assays indicated that BDNF secretion was significantly greater than NT3 secretion, as anticipated from the latter being downstream of the IRES element.

This dual neurotrophin-encoding plasmid extended the previously validated efficacy of GET driving BDNF expression for rapid auditory nerve regeneration[11] with the addition of the NT3 expression element, which is known to have substantial trophic activity in the cochlea acting synergistically with BDNF treatment to enhance auditory nerve regeneration.[24] In vivo delivery parameters for pFAR4-CMVp-BDNF-NT3 DNA were matched to the pFAR4-CMVp-eGFP study, with equivalent voltages achieved (Table S1, Supporting Information; mean current amplitude for four deafened guinea pigs = 30.8 ± 2.92 mA, to achieve a maximum applied voltage of 120 V for DNA delivery). The readout from these experiments included ELISA quantitation of BDNF and NT3 levels in cochlear perilymph 2 weeks post-CC-GET (1 month after deafening), PCR screening for residual recombinant plasmid DNA in tissues (brain, heart, blood, mastoid process muscle, liver, kidney, stool, and urine), which did not detect the transgene DNA in any of the tissue samples, and immunofluorescence imaging of the spiral ganglion in cryosectioned cochlear tissue. In the four deafened guinea pigs the pFAR4-CMVp-BDNF-NT3 DNA CC-GET – treated cochleae showed ≈3x higher BDNF levels than the corresponding baseline levels in the untreated cochleae (Figure S5, Supporting Information) (control = 565 ± 396 pg mL$^{-1}$ BDNF; neurotrophin DNA treated cochleae = 1674 ± 356 pg mL$^{-1}$ BDNF; $p$ = 0.0189, two-tailed paired $t$-test). There was no significant difference between NT3 levels across treated and untreated cochleae (control = 162 ± 64 pg mL$^{-1}$ NT3; neurotrophin DNA treated cochleae = 165 ± 43 pg mL$^{-1}$ NT3; $p$ = 0.941, two-tailed paired $t$-test).

Confocal immunofluorescence validated the effectiveness of the therapeutic neurotrophin-encoding miniplasmid in regenerating the peripheral neurites of the spiral ganglion in the deafened guinea pigs, where TUBB3 ($\beta$3Tubulin) immunofluorescence intensity in the osseous spiral lamina (OSL) region was compared with batch-processed untreated opposite cochleae (**Figure 5**a–c). Dense fascicles of spiral ganglion neurites were evident in the cochleae receiving the neurotrophin gene augmentation, while the untreated cochleae showed a paucity of fibers,

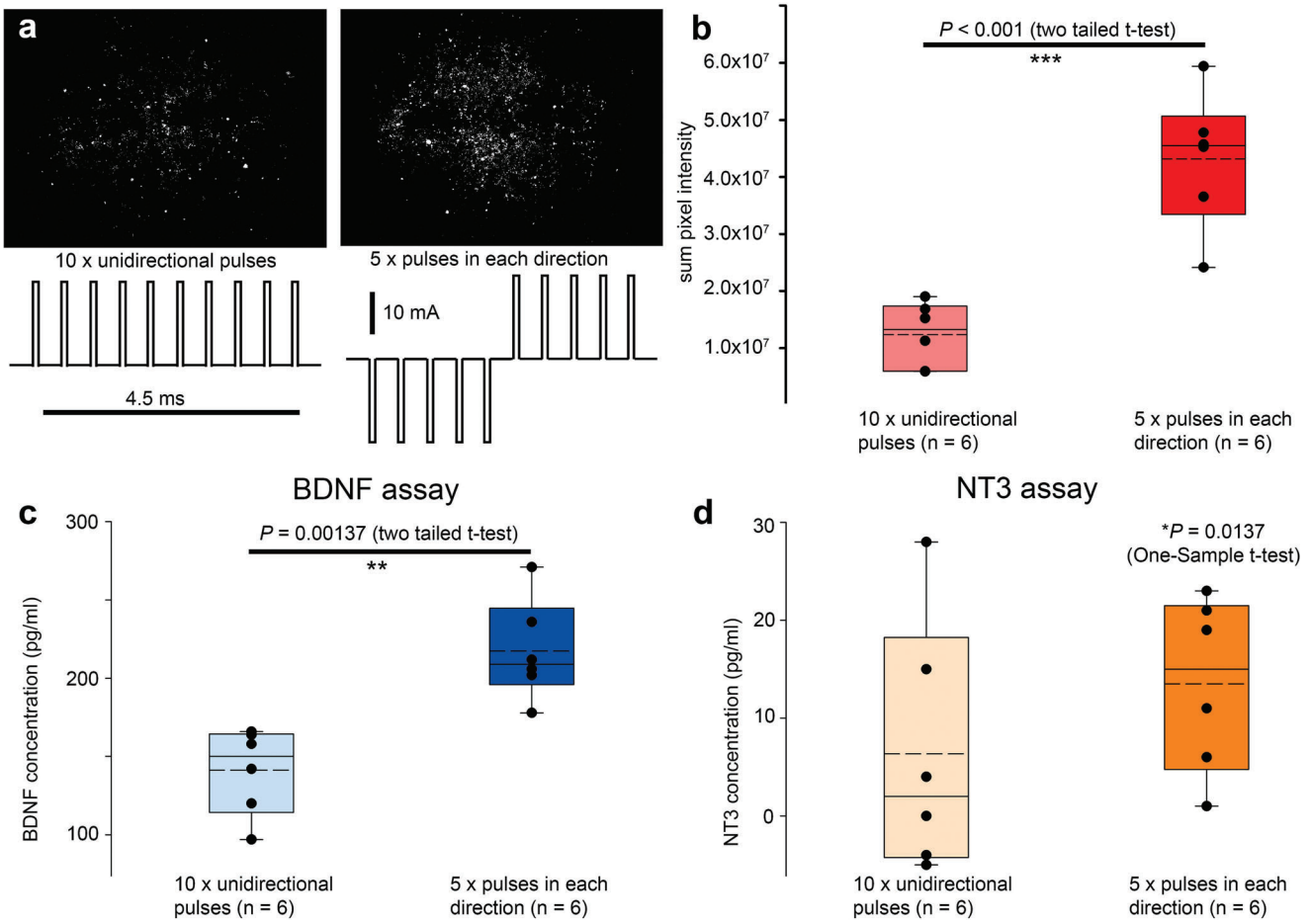


**Figure 4.** Validation of recombinant BDNF and NT3 protein synthesis using HEK293 cells and the clinical CC-GET device to deliver pFAR4-CMVp-BDNF-NT3 miniplasmid and pBs-CMVp-mCHERRYnls reporter DNA. a,b) Comparison of mCherry reporter expression using positive-going, versus positive then negative pulses for GET (100 µs × 20 mA; 400 µs interpulse interval). c,d) Validation of BDNF and NT3 secretion using both pulse train profiles. Data reflected in Figure 12 Patent ref. [23]. Cells were imaged and supernatant was collected for ELISA at 4 days post CC-GET. See also Supporting Information – Methods and Primary Figure Commentary.

consistent with the deafening procedure. The average pixel TUBB3 immunofluorescence intensity in the region of interest (distal 50% of the OSL) of the neurotrophin DNA – treated cochleae was 816.7 ± 61.5, compared to 537.7 ± 48.1 for the untreated control cochleae ($p = 0.0160$, Student's paired *t*-test, one-tail) (Figure 5d). In addition, there was a pronounced increase in TUBB3 immunofluorescence in the SGN soma region, reflecting increased translation of the neurofilament protein associated with neurite outgrowth.

### 2.6. Preclinical validation of Long-Term Stability of the Neurotrophin CC-GET-Enhanced Bionic Interface in the Deafened Cat Model

Prior studies in cat and guinea pigs have shown that BDNF-mediated regeneration of cochlear auditory neurites, albeit with promiscuous outgrowth, can be maintained using chronic stimulation via a CI,[25,26] whereas without electrical stimulation, the neurites regress when intracochlear BDNF infusion ceases.[27] To evaluate the ability of chronic CI use to promote long-term stability of the neurotrophin CC-GET – enhanced bionic interface, a 6-month longitudinal study of deafened cats was undertaken. The cat cochlea model benefits from the close anatomical semblance with humans, particularly in the basal half of scala tympani.[19] This accommodates the transient insertion of zone 1 of the clinical CC-GET array (electrodes 22–15). Additionally, these animals are able to utilize bilateral CIs for hearing, with associated external speech processors and battery packs accommodated in a jacket, to sustain chronic electrical stimulation.

Validation of efficient CC-GET was initially undertaken in one normal-hearing cat using pFAR4-CMVp-eGFP reporter DNA, bilaterally, with fixation of the cochleae after 72 h (**Figure 6**a,b). These data confirmed that the current pulse profile optimized in the guinea pig study (10 × 100 µs × 50 mA) was effective in cats, and therefore likely to be appropriate for human cochlear gene augmentation treatment. In the pFAR4-CMVp-eGFP reporter-expressing cat cochleae, the GFP-labeled mesenchymal cells were confined to scala tympani in the basal half of the cochlea, and the highest density of cells was at the basal mid-turn region, distal from the round window membrane. This demonstrated site-specific control of the gene electrotransfer matched to the electric

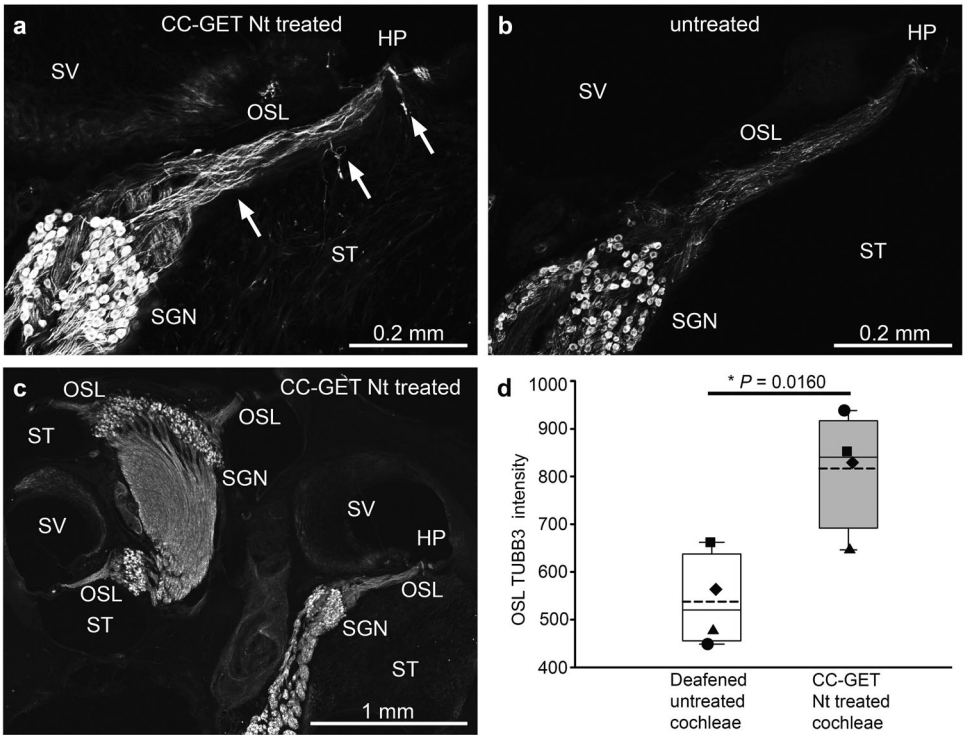


**Figure 5.** CC-GET delivery of the clinical pFAR4-CMVp-BDNF-NT3 miniplasmid DNA drives cochlear spiral ganglion neuron (SGN) regeneration in deafened guinea pigs. a) Detail of basal cochlear region showing neurite outgrowth (TUBB3 immunofluorescence) following neurotrophin-encoding DNA electrotransfer. Arrows indicate ectopic growth of the spiral ganglion neurons (SGN) into scala tympani (ST). b) Untreated opposite cochlea from the same animal showing atrophied SGNs in the same region. c) Low power mid-modiolar image from (A), showing higher intensity immunofluorescence of the neurites in the osseous spiral lamina (OSL) in the more basal region. d) SGN neurite fluorescence signal (mean pixel intensity) within the distal half of the basal region OSL; 25% and 75% boundaries with 95% limits; individual data from 4 animals at 2 weeks post CC-GET. Student's paired *t*-test, one-tail. HP – habenula perforata, SM – scala media, SV – scala vestibuli.

field profile established for zone 1 of the clinical CC-GET device (peak electric field density ≈e19–e18).

Having validated CC-GET in the cat cochlea using eGFP reporter expression, delivery of pFAR4-CMVp-BDNF-NT3 DNA to one cochlea and pFAR4-CMVp-eGFP reporter-encoding DNA (control) to the opposite cochlea, was undertaken in four cats deafened 1–3 months prior to surgery. Immediately after the electrotransfer current pulse train, the clinical CC-GET device was withdrawn and replaced with a 14-electrode CI array controlled by an externalized connector-coupled Cochlear Nucleus 5 Sound Processor stimulator (Cochlear Ltd.). Thus, the only difference in treatment between the left and right cochleae in each cat was the DNA sequence (randomized and blinded). The DNA electrotransfer utilized a current-controlled pulsed electric field equivalent to that determined for the preceding guinea pig and cat experiments (Table S2, Supporting Information). Overall, across ten cat cochleae, the average current delivered by 10 × 100 µs pulses for CC-GET was 34.1 ± 1.6 mA (1 ms combined pulse duration), affording an average charge transfer of 34 µC, via a mean applied voltage of 117.5 ± 2.5 V. On average the clamped resistance equated to 3.55 ± 0.24 kΩ.

The CI arrays were switched-on 2 weeks postsurgery, and three cats used these devices continuously for hearing for 135–159 days. Functional assessments were performed periodically to measure neural recruitment thresholds from electrically evoked compound action potential (eCAP) recordings (Figure S6, Supporting Information). These data, elicited using monopolar (MP+1) stimulation along the length of the CI array, with recording from adjacent electrodes, showed maintained thresholds of equivalent sensitivity in the auditory nerve across cochleae for both control pFAR4-CMVp-eGFP and neurotrophin-encoding pFAR4-CMVp-BNDF-NT3 DNA CC-GET. At the 6-month endpoint, the cats were anesthetized to enable mapping of inferior colliculus neural recruitment via electrical stimulation of the CI arrays for the CC-GET neurotrophin-treated cochlea and the CC-GET-eGFP-treated (control) cochlea for each cat. No systemic dispersion of the pFAR4 DNA was detectable by polymerase chain reaction (PCR) analysis in organs, blood, and urine samples (Supporting Information–Methods).

In all three cats, immunofluorescence labeling of fixed, decalcified, and cryosectioned cochleae that had received the CC-GET neurotrophin gene augmentation treatment 6 months prior, showed the anticipated retention of spiral ganglion neurite regeneration within the osseous spiral lamina projecting in close proximity to the CI array. Consistent with tropic guidance from mesenchymal cell BDNF-NT3 production, regenerated neurites projected out of the osseous spiral lamina into the proximal aspect of scala tympani, as well as extending past the normal insertion point at the habenula perforata to the lateral spiral ligament, penetrating to the mesenchymal cell lining (Figure 6c–e). The fibrotic

 

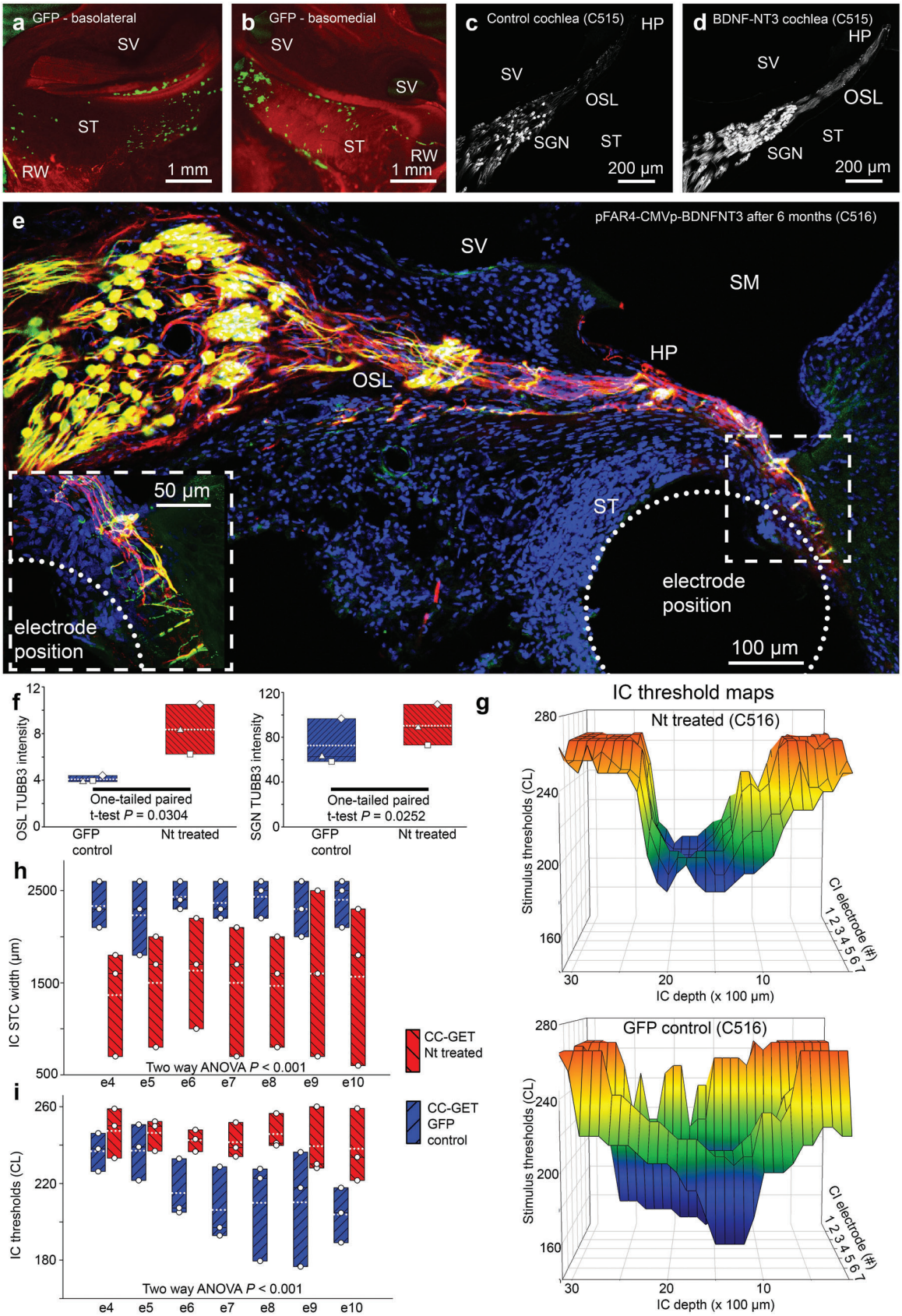

infiltration around the CI array evidently acted as a support matrix for the spiral ganglion neurite projections which ended in fine processes within ≈20 µm of the electrodes (Figure 6e inset). This confirmed that the "neural gap" with the CI array could be minimized using the pFAR4-CMVp-BDNF-NT3 neurotrophin CC-GET technology and that this benefit was maintained with the use of the CI. Tubulin beta 3 class III (TUBB3) immunofluorescence intensity in the peripheral neurites in the osseous spiral lamina was significantly higher in the neurotrophin CC-GET-treated cochleae, (neurotrophin-DNA = 8.35 ± 1.23; eGFP-DNA = 4.08 ± 0.17; $p = 0.0304$, one-tailed paired *t*-test; Figure 5f; Figure S7, Supporting Information). Similarly individual spiral ganglion soma showed significantly increased levels of this microtubule protein in the neurotrophin DNA-treated cochleae compared with cochleae receiving the pFAR4-CMVp-eGFP DNA (mean pixel intensity NT DNA = 90.39 ± 10.54, eGFP DNA = 72.59 ± 12.13; $p = 0.0252$; one-tailed paired *t*-test; Figure 5g; Figure S7, Supporting Information). Consistent with neuroprotection associated with neurotrophin treatment,[26] the average number of soma in the basal region trended higher in the neurotrophin-DNA treated cochleae compared with the GFP control cochleae (NT DNA group = 38.33 ± 11.86 neuron soma / SGN ROI; eGFP DNA group 21.25 ± 7.52; $p = 0.118$, one-tailed paired *t*-test; $n = 3$ cochleae, each a mean of 4 SGN ROIs/group; Figure S7, Supporting Information).

Imaging failed to detect expression of the eGFP reporter in the control-side cochlea from each of the cats in the long-term study, consistent with a fall-off in transgene expression demonstrated in the guinea pig due to turn-over of the transfected mesenchymal cells.[17] Thus, the retention of regenerated peripheral spiral ganglion neurites arising from a limited period of recombinant BDNF and NT3 expression by the scala tympani mesenchymal cells was most likely achieved through complementary chronic electrical stimulation via the CI. The key differential here is the directed regrowth of the auditory dendrites to the vicinity of the CI electrodes achieved by targeted neurotrophin CC-GET to the mesenchymal cells proximal to the CI array.

The functional effect of the neural enhancement of the CI interface was validated at the 6-month endpoint by analysis of spatial tuning curve (STC) widths within the inferior colliculus, recorded under anesthesia using a 32-channel linear recording array placed in either hemisphere of the IC, and stimulated by both CI arrays using a bipolar stimulation modality, for CI electrodes e4–e10. There was a significant sharpening of the STCs driven by neurotrophin-treated cochlear input, compared with stimulation via the opposite control cochlear input (Figure 6g–i; Figure S8, Supporting Information). The average STC width with neurotrophin CC-GET across all 32 IC electrodes driven by 7 CI electrodes was 1519.0 ± 131.6 µm, compared with 2357.1 ± 51.0 µm for the eGFP CC-GET control cochlear input ($p < 0.001$, two-way ANOVA) (Figure 6h). This reflects a broad hyperexcitability (lower thresholds) within the IC in response to stimulation of the control cochlear input, whereas the neurotrophin-treated cochlear drive was more spatially specific. The average threshold across all 32 IC electrodes, driven by the seven control CI electrodes was 217.04 ± 4.66 current level (CL), compared with 243.00 ± 2.43 CL for input from the 7 CI electrodes from the neurotrophin-treated cochleae ($p < 0.001$, two-way ANOVA) (Figure 6i). CL is defined by Cochlear Ltd. where, current in µA = 17.5× (100 ^ (CL/255))

### 2.7. CC-GET Enables Targeted In Vivo Gene Delivery Within the Brain

The utility of CC-GET using the bionic array-based electric field focusing on targeted brain DNA therapeutics was evaluated by in vivo plasmid DNA delivery in guinea pigs. These studies, utilizing nine animals, evaluated expression of a range of reporter constructs, including a tdTomato tagged red-shifted channel rhodopsin ion channel under the human synapsin (hSYN) promoter (ReaChR; pJL-hSYNp-ReaChR-tdTomato; Figure S1E, Supporting Information), and the cytomegalovirus promoter (CMVp)-driven GCaMP5g $Ca^{2+}$ reporter (pAG-CMVp-GCaMP5g; Figure S1F, Supporting Information). GFP reporter plasmid DNA (pFAR4-CMVp-eGFP) was delivered to two sites, the dorsomedial brainstem (nucleus of the tractus solitarius, NTS), and the globus pallidus (GP), deep thalamic region. A second reporter plasmid pMK-CAGp-eGFP (Figure S1G, Supporting Information) was delivered to the NTS. The GP brain region is a target for deep brain stimulation bionics to manage debilitating motor symptoms in Parkinson's disease. Gene augmentation to achieve expression of recombinant ion channels at this site is likely to provide therapeutic neuromodulation. Proof of concept for such targeted neuromodulation was established utilizing CC-GET to achieve light-pulse activation of GP neurons expressing ReaChR channels, altering $Ca^{2+}$ transients, recorded as changes in GCaMP5g fluorescence in brain slices.

GFP reporter expression was achieved across both brain region targets (**Figure** 7a–c). Overall, CC-GET provided highly reliable gene expression (4/4 animals). The choice of the NTS brainstem region, critical for cardio-respiratory function, validated the CC-GET safety profile. CC-GET was well tolerated with no adverse indicators evident across the 3–7 days until predetermined

**Figure 6.** Clinical CC-GET neurotrophin gene augmentation with chronic cochlear implant (CI) stimulation achieves long-term rescue of regenerated spiral ganglion neurites and reset of central auditory tuning in the cat inferior colliculus. a,b) Targeting of perilymphatic mesenchymal cells in the basal scala tympani (ST) region confirmed by pFAR4-CMVp-eGFP reporter expression; adjacent scala vestibuli (SV) is unlabeled; the GET probe was inserted via the round window (RW) membrane. c,d) Comparison of CC-GET of control eGFP reporter DNA C), versus pFAR4-CMVp-BDNF-NT3 DNA D) shows long-term rescue of spiral ganglion neurites (TUBB3 immunolabeling) within the osseous spiral lamina (OSL), supported by sustained (≈6 months) electrical stimulation via the CI. e) Detail of projection of rescued auditory neurites to the region of the CI "closing the bionic interface neural gap" (TUBB3/neurofilament 200 immunolabeling). f) Quantitation of anti-TUBB3 fluorescence intensity in the OSL region and spiral ganglion neuron somata (SGN) from cryosections (symbols distinguish average data from the three cats). g) Sharper spatial tuning curve (STC) threshold profile recorded through a region of the inferior colliculus driven by the CI in the neurotrophin CC-GET – treated cochleae (top) compared with input from the control eGFP DNA-treated cochlea (bottom). h) Spatial tuning curve (STC) widths and i) average stimulus thresholds, show that the cochlear neurotrophin gene augmentation treatment results in an overall reduction in excitability, associated with sharpening of spatial tuning. See also Supporting Information – Methods and Primary Figure Commentary.

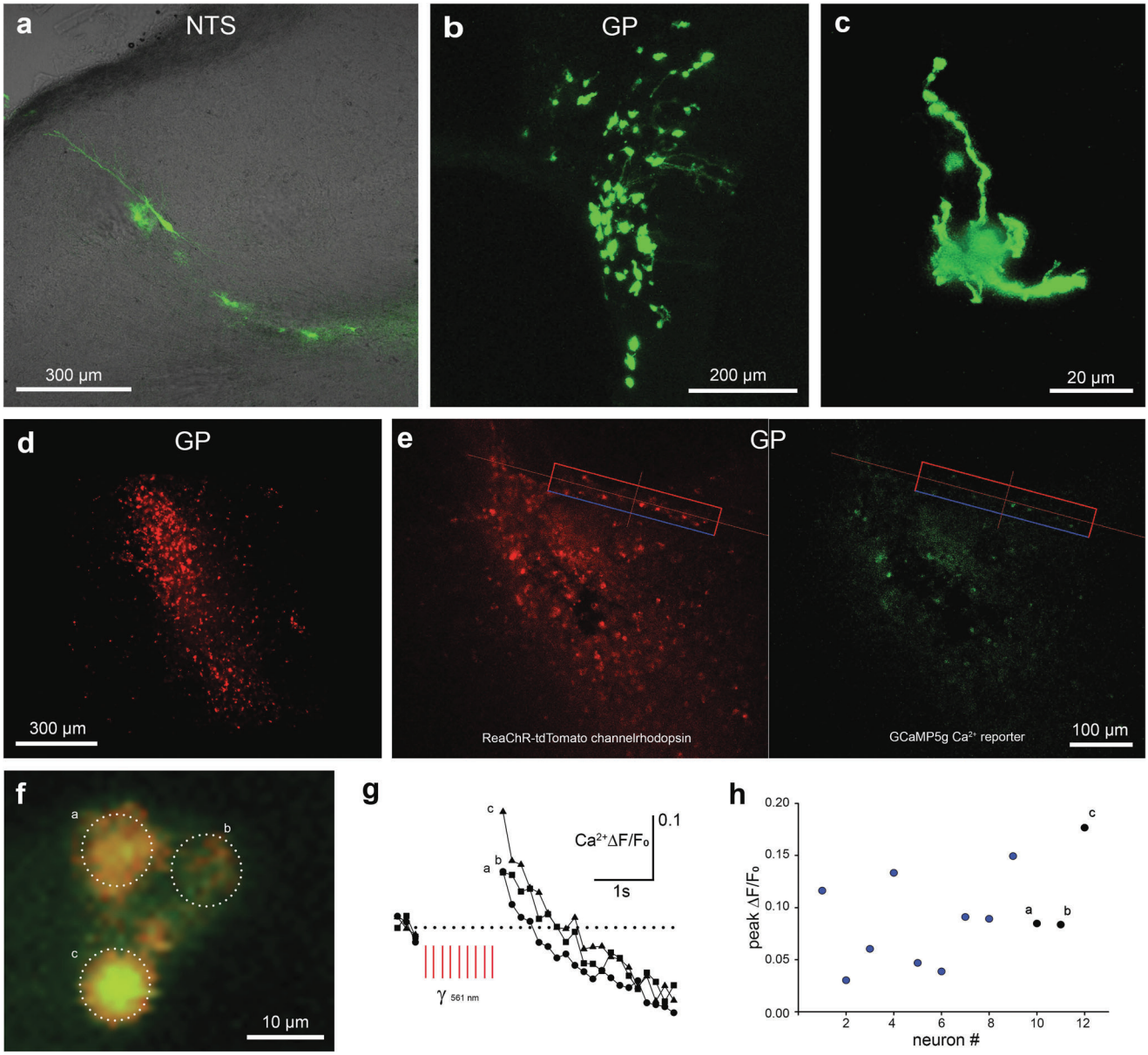


**Figure 7.** CC-GET gene delivery to the guinea pig brain achieves targeted optogenetic neuromodulation. A) pFAR4-CMVp-eGFP plasmid DNA delivery to the nucleus of the tractus solitarius (NTS) region of the brainstem. B,C) pMK-CAGp-eGFP plasmid DNA delivery to the globus pallidus (GP). D,E) Dual delivery of pAG-CMVp-GCaMP5g $Ca^{2+}$ reporter + pJL-hSYNp-ReaChR-tdTomato channel rhodopsin plasmid DNAs to GP region (10 × 100 µs × 50 mA pulses). F) Detail of three neurons co-expressing ReaChR and GCaMP5g. G) $Ca^{2+}$ responses to 561 nm pulsed laser activation of ReaChR channels in the three neurons shown in (F). H) Peak $Ca^{2+}$ responses for 12 neurons. Images from (B) and (C) are from patent ref. [16]. See also Supporting Information–Methods and Primary Figure Commentary.

endpoint. This was supported by the postmortem integrity of brain parenchyma in the regions showing GFP expression in neurons (Figure 7a). These studies demonstrated substantial populations of transfected neurons within both regions (Figure 7a,b). The flexibility of CC-GET for delivery of cocktails of plasmid DNAs was validated by bilateral targeting of the GP with a combination of pAG-CMVp-GCaMP5G DNA and pJL-hSYNp-ReaChR-tdTomato. Both plasmid DNAs achieved neuron-selective expression, where ReaChr was detected via its fused tdTomato reporter ($n = 5/5$) (Figure 7d–f). ReaChR expression enabled optogenetics-based neuromodulation of individual GP neurons in brain slices, where GCaMP5g co-expression reported $Ca^{2+}$ dynamics evoked by 561 nm light-activation (0.3–1.2 s) (Figure 7g,h). Overall, the peak GCaMP5g $\Delta F/F_o$ intracellular $Ca^{2+}$ signal after cessation of the red light stimulation was $0.0918 \pm 0.0131$ above the preceding baseline (3 sample average; $p = 0.0000223$, one sample $t$-test, $n = 12$ neurons/7 slices).

Table S3 (Supporting Information) provides the current amplitude (range 10–50 mA) and delivered voltages (range 25–90 V) for 10 × 100 µs pulses or 3 × 100 ms pulses for brain CC-GET, and

calculated local resistance determined across the gene delivery array in the presence of plasmid DNA in sucrose carrier. The effectiveness of controlling local brain conductivity was evaluated by comparing resistance measured across the clinical CC-GET electrode array at baseline (no DNA present), against measurements at the time of GET. Resistance increased by 138% (1.08 ± 0.08 kΩ baseline ($n = 11$) to 2.58 ± 0.29 kΩ ($n = 8$); $p = 0.0000282$; $t$-test). This reduction in local brain conductivity would significantly increase the focal electric field intensity in the region adjacent to the gene delivery array (as shown in Figure 1), and hence drive efficient electrotransfer of the plasmid DNAs.

### 2.8. Context of CC-GET Development for Targeted Gene Expression in the Nervous System

The current study advances the translational platform for discrete gene electrotransfer-based therapeutics within nervous system tissues, demonstrating the utility of electric field focusing achieved via variable configuration of a linear array of electrodes, augmented by suppression of local tissue conductivity ("conductivity-clamping"). Development of the clinical CC-GET device gene delivery electrode array enabled precise control of the tissue volume for gene expression of the naked (plasmid) DNA gene payload. The "electro-lens" effect to expand, or contract, the field of transfected cells was achieved by changing the separation of the linear cathode and anode electrode elements. Local control of tissue conductivity by displacement of the physiological ionic milieu with nonionic sucrose carrier biased the local current flow between the CC-GET probe electrodes to the polyanionic DNA species, amplifying local electric field strength for a given charge delivery.

The local extracellular (field) voltage provides the driving force for DNA transfer, but central to this is the change in voltage with distance (electric field strength) at the cellular level. In our in vitro HEK293 cell modeling, the threshold for plasmid DNA CC-GET was ≈120 V cm$^{-1}$ (Figure 2). The linear electrode array used for close-field CC-GET maximizes this local field potential gradient, evident from the electric field maps, where field strength can be maximum close to the null point (zero voltage) zone between the anodes and cathodes (Figure 2 and ref. [12]). With conventional open field GET, because of the relatively high extracellular tissue conductivity, a large amount of current is needed to achieve suprathreshold field strengths. Examples include applications across a range of clinical electroporation devices driving multi-electrode configurations for intradermal delivery of plasmid DNA vaccines subcutaneously, requiring 400–500 mA with pulse widths of 52–60 ms (reviewed by Broderick and Hueau[28]); equivalent to ≈25 mC of charge per pulse (2–3 pulses). Such high current fluxes lead to tissue damage associated with local ohmic heating and irreversible electroporation.[18] This was illustrated in the present study with delayed application of propidium iodide following GET with saline carrier at 3 × 100 ms × 35 mA pulses (10.5 mC), where the HEK293 cells exhibited fluorescence in a margin adjacent to the gene delivery array placement.

Across studies involving electroporation-mediated DNA vaccine delivery to hundreds of human subjects, pain is a notable side-effect, taking several minutes to subside.[28] In comparison, the threshold charge delivery per pulse for CC-GET incorporating the sucrose carrier (3 × 5 mA × 100 µs pulses in HEK293 cell monolayers, as shown in Figure S3, Supporting Information; US patent ref. [16]), was 0.5 µC per pulse (50 000 times less charge). For perspective, this is only marginally greater than the charge delivered per pulse in CI devices at continuous neural stimulation at rates in the kHz range for routine hearing prosthesis function.[29] The CC-GET refinements applied in vivo achieved functionally comparable gene expression in the cochlea at ≈1000-fold less charge compared with the original bionic array-based close-field GET study by Pinyon et al.[11] This speaks to the efficiency and safety of the CC-GET technology. Further, the GET of plasmid DNA is highly permissive with regard to packaging size, with the present study demonstrating high expression efficacy across seven plasmids ranging in size from 2.83 to 7.68 kb, in the MDa range.

### 2.9. Translational Pathway for Clinical CC-GET-Mediated Neurotrophin Gene Augmentation to Enhance Bionic Hearing

The CC-GET probe included micro-fluidics for delivery of the humanized bicistronic expression cassette encoding the BDNF & NT3 genes within a pFAR4 miniplasmid, eliminating the potential for dissemination of antibiotic resistance genes associated with standard plasmid vectors, and satisfying the European Medicines Agency requirements for GET.[21] The delivery of this therapeutic DNA and sucrose formulation via insertion of the CC-GET device probe through the cochlear round window displaced the perilymph, reducing local conductivity in the tissue around four-fold across guinea pig and cat experiments, with commensurate reduction in the electric current levels needed to achieve a therapeutic level of gene expression. As such, the capability of CC-GET for gene augmentation applications was advanced to a clinic-ready technology aiming to improve hearing outcomes in CI recipients by using precise delivery of neurotrophins directing auditory nerve regeneration toward the CI array, closing the neural gap and thereby improving the bionic interface.

The safety and efficacy of the CC-GET neurotrophin treatment in the cochlea was validated in vivo in the deafened guinea-pig model, demonstrating rapid regeneration of the auditory nerve, while the chronic studies in the neonatally-deafened cat model validated the long-term safety and viability of the treatment. This outcome highlights the broad potential for neurotrophin-based CC-GET to regenerate peripheral nerves. These studies, along with subsequent good manufacturing practice (GMP) production of the clinic-ready CC-GET device, and the humanized neurotrophin-encoding DNA therapeutic molecule, supported the registration of a first-in-human phase I/IIa clinical trial of neurotrophin CC-GET gene augmentation treatment during CI surgery through the Australian Therapeutic Goods Administration[30] (currently underway). It is notable that gene augmentation treatments using (biologically inert) naked DNA are not subject to gene technology regulatory oversight in Australia, but rather lie within the conventional medical device-small molecule therapeutics clinical trial framework.

The use of this CC-GET device to deliver the pFAR4-BDNF-NT3 miniplasmid resulted in highly reproducible directed regeneration of the cochlear auditory nerve fibers in both animal

models. Thus, the key benefit here of the CC-GET targeted delivery to the cochlear mesenchymal cells adjacent to the subsequently implanted CI array is the establishment of a local tropic signaling gradient where recombinant BDNF is able to establish guidance via the activation of its cognate neurotrophic tyrosine kinase receptor type 2/TRKB receptor on the spiral ganglion neurons, with likely downstream signaling via $G_{\alpha q}$- phospholipase C$\gamma$ (PLC$\gamma$)- phosphotidylinositol 4,5-bisphosphate ($PIP_2$)- diacylglycerol (DAG) second messenger signaling of canonical transient receptor potenital 3 (TRPC3) channels,[31] which are known to be expressed by the SGNs.[32] The CC-GET-mediated recombinant BDNF production is likely to have dominated the spiral ganglion neurite regeneration, as this was most effectively secreted in the in vitro HEK293 cell model, and BDNF levels in the bulk guinea pig perilymph samples of the neurotrophin-CC-GET study were four times higher than the background, while the perilymph NT-3 levels in vivo were not significantly greater than the untreated cochlea reference level. In the cochlea, the sensory hair cells are the principal source of BDNF.[33] NT3 is associated with the supporting/glia-like cells in the cochlea, alongside inner hair cells, and facilitates auditory synapse recovery after noise trauma in the basal (high-frequency) encoding region.[34,35] The deafening procedure leads to the loss of these organ of Corti sensory hair cells and supporting cells, disrupting BDNF/NT3 production, leading to retraction of the SGN neurites and atrophy of the somata, while the centrally connected auditory axons remain viable, albeit with some SGN loss.

The SGN nerve regeneration was transient in the deafened guinea pigs. This most likely arose from fall-off in the recombinant neurotrophin secretion as the targeted mesenchymal cells lining the scala media compartment turned-over.[17] In previous cat and guinea-pig studies, chronic electrical stimulation via the CI devices achieved maintenance of BDNF-infusion-retrigerated cochlear spiral ganglion neurites.[25,36] A key distinguishing feature of preceding deafened cochlear preclinical studies using direct infusion, or viral-vector-mediated delivery of BDNF or NT3, was the unintended ectopic over-extension of the neurites that occurred.[25,37,38] This can thwart the utility of CIs, where local stimulation of sub-populations of nerve fibers is required to match the tonotopic mapping of the cochlea that underlies pitch perception. In the present study, the spiral ganglion neurite outgrowth was discrete, and with chronic stimulation via the CI in the cat model, the fibers remained in close proximity (<20 µm; Figure 5e) to the electrode array for the ≈6-month duration of the study. This enhanced neural interface significantly reset spatial tuning within the inferior colliculus.

The plasticity of the auditory brainstem pathways underpins the restoration of hearing with the "bionic ear."[39] In the deafened cat model, it has been reported that with deafening, with or without chronic electrical stimulation via a CI, intrinsic plasticity in the primary auditory cortex lends broad zones of activation, associated with local circuit disinhibition.[40] In the inferior colliculus of adult cats, the STC widths broaden with deafening, and to an even greater extent in neonatally deafened cats,[41] the model used in the present study. Nonspecific chronic electrical stimulation via the CI can cause further de-tuning of the cochleostomy at this level.[41] In the present study, the cats experienced sustained use of their bilateral CIs (with and without the neurotrophin gene augmentation), with clinical speech processors enabling environmentally relevant sound encoding and communication for many months. This natural dynamic auditory stimulation is evidently matched to the restoration of central auditory circuit functionality, where with the improvement of the neural interface as a result of neurotrophin gene augmented CI treatment (enhanced auditory drive), there was a significant rescue of spatial mapping of hearing coding, which would support upstream improvement in thalamic and cortical auditory circuit performance. This may be at the local synaptic level within the inferior colliculus, where the contralateral drive to the same neural field via the cochlea receiving only the eGFP control DNA exhibited broad STC widths. This contributes insight into the plasticity of central auditory processing that likely underpins the progressive improvement in hearing performance that occurs in the months following CI surgery.[42]

### 2.10. Extension of CC-GET to Precision Gene Transfer Targeting Within the Brain

Gene therapy in the broadest sense of DNA/RNA-based therapeutics is increasingly being pursued to address CNS neurological disorders.[43,44] The extension of the utility of CC-GET-based focal gene augmentation to brain therapeutics was demonstrated by targeted gene expression across a range of guinea pig brain regions and validation of targeted neuromodulation via optogenetics. Currently, there are more than 179 active studies in clinical trials for CNS disorders, including a lentiviral vector-based study for drug-resistant intractable epilepsy and more than ten lentiviral and AAV-2-based gene therapy clinical trials directed to Parkinson's Disease (PD).[45,46] Contrasting with the limited spatial targeting of viral vector-based gene delivery due to sustained transduction activity as viral particles disperse, pulsed electric field-based "naked" DNA electrotransfer using conductivity-clamping has the evident potential, clearly validated here, to achieve superior spatial control of gene expression and resolve these other challenges, as well as being cost-effective and faster to implement. However, no CNS gene therapy clinical trials have adopted clinical electroporator-based gene transfer; reflecting the incompatibility of electrode invasiveness in clinical GET devices, and the tissue-damaging current pulses and associated charge transfer needed for DNA electrotransfer with those devices. Across brain regions, in cases where plasmid DNA-based gene expression has been achieved in vivo in the adult mammalian brain via GET, "micro-electroporation" has achieved limited neuronal expression across a range of brain regions in preclinical models, utilizing single or paired needle electrodes. This includes lateral geniculate nucleus targeting in mice and cats,[47] suprachiasmatic region in hamsters,[48] dual small interfering RNA (siRNA) and plasmid reporter DNA delivery into rat anterior cingulate cortex.[49] It is notable that brain electrolytic lesions are reported in the region of the GET, particularly close to the electrodes (highest field strength zone) at high voltage–current levels.[47,50] Use of closely apposed electrophysiology recording electrodes, as GET electrodes, stereotaxically positioned within the mouse hippocampus enabled delivery of a $\beta$-galactosidase reporter plasmid (saline carrier with low current pulses; 125 µA x 50 ms; 6 µC charge), consistently achieving small fields of transformed neurons.[51] A similar approach using a single electrode with a needle as the anode return as well as

providing local delivery of a range of plasmid DNAs, achieved consistent focal expression within neurons, or astrocytes (DsRed reporter driven by a glutamate-aspartate transporter (GLAST) promoter) within the striatum in adult mice, with low voltage pulses (25–35 V × 50 ms). Minimum tissue injury was observed outside of the immediate region of the electrode and delivery needle. These preceding studies highlight the requirements for low current amplitudes and local delivery of the DNA for focal GET in the brain.

In the present study, the combination of electrode array-based electric field "lens" focusing and conductivity – clamping enabled the clinical CC-GET device to achieve highly reproducible targeted delivery of plasmid DNAs to transduce substantial fields of neurons within the adult guinea pig brain. The inclusion of microfluidics to deliver the sucrose-based non-ionic carrier and plasmid DNA within the suprathreshold electric field to locally reduce conductivity and thereby amplify the electric field was effective, as the resistance in the close-field was increased by 138%.

The dual neuronal expression of plasmid DNAs encoding red-shifted channel rhodopsin (ReaChR) and the GCaMP5g $Ca^{2+}$ reporter in the globus pallidus brain region enabled "proof of concept" for optogenetics-based neuromodulation. In PD, this is the site of hyperactivated premotor neurons, due to disinhibition through loss of dopaminergic substantia nigra input.[46] Current management of the PD-associated movement dissociation (dyskinesia) includes the use of bionic array-based DBS, as the standard of care for patients associated with loss of effectiveness of L-DOPA treatment.[52] DBS uses cochlear implant-like electrode arrays to provide continuous stimulation to suppress neuronal activity within the globus pallidus internus and subthalamic nuclei (where for example, the device may operate at up to 250 Hz with 25 mA × 450 µs pulses (≈11 µC of charge per pulse),[20,53] which for perspective, is >20× the CC-GET threshold). Based on the findings from the present study, spatially-controlled CC-GET could be used to safely target this brain region for neuromodulation via recombinant ion channel expression, to complement or replace DBS, including the use of optogenetics strategies in combination with bionic arrays (a feature emerging in the CI field).[54,55] Alternatively, emerging technologies for intrinsic regulation of gene dose of recombinant $K^+$ channels, such as demonstrated preclinically in a DNA therapeutics model for epilepsy utilizing Kv1.1 channels,[56,57] could broadly enable neuromodulation via CC-GET to treat focal neurological disorders and brain pathophysiology. CC-GET could also enable local expression of neurotrophins, particularly BDNF, which provide neuroprotection from the subacute phase of secondary brain injury expansion following stroke.[58] Such approaches may be extended to RNA-based therapeutics, which would address the necessity to manage the duration of treatment in neurons, which being terminally differentiated, could potentially express therapeutic plasmid DNAs indefinitely. DNA therapeutics engaging immunological mechanisms are also emerging for brain disorders. Preclinical in vivo models using AAV delivery of interleukin 2 encoding DNA in the brain stimulate the expansion of resident regulatory T cells that suppress neuroinflammatory responses associated with stroke, traumatic brain injury, multiple sclerosis, and cognitive decline.[59,60] There is also clear potential to develop CC-GET to achieve recombinant cytokine expression targeting intratumoral therapeutics for brain tumors such as glioblastoma multiforme (GBM). Such DNA/RNA therapeutics are relevant to the broad range of GBM treatment options currently in preclinical evaluation, or clinical trial, including viral vector-delivered suicide genes such as thymidine kinase, and the use of vascular endothelial growth factor receptor proteins to inhibit tumor angiogenesis (reviewed by refs. [61, 62]).

## 3. Conclusion

The technical development and translational pathway for the clinic-ready CC-GET medical device is outlined here. The precision delivery of a human-gene therapy optimized plasmid DNA encoding the BDNF and NT-3 neurotrophins to the cochlea in deafened animal models drove auditory nerve regeneration that achieved sustained improvement in hearing performance with cochlear implants. This established the case for clinical trial registration for a first-in-human phase I/IIa study. The biophysical properties of the conductivity-clamping enhanced focused electric field GET were found to match the needs for focal brain therapeutics. The CC-GET technology provided control of DNA delivery titer, matched to targeted spatial expression mapping, brain cell-type selectivity, safety, and durability. Proof of concept was achieved for photonics-based neuromodulation via channelrhodopsin expression in a brain region relevant to the treatment of Parkinson's disease. This capability aligns with the unmet need for treatment of a range of focal neurological disorders and brain oncology applications. Overall, there are evident advantages to CC-GET-based gene delivery, these include a lack of size constraints on gene construct packaging, and a lack of immunogenicity of naked DNA, which is a major drawback of viral vector-based delivery. This provides an improved safety profile and lowered regulatory barriers, with faster and lower-cost development. The key feature of instantaneous "fixing" of the field of gene expression to the brief period of delivery of the pulsed electric field overcomes the challenge inherent to other gene delivery systems. These properties are ideal for targeted gene delivery across the central and peripheral nervous systems, and muscle, and a breadth of emerging applications for nucleic acid-based gene therapeutics. While the current clinical CC-GET device design is adapted to provide flexible conformation to soft tissue targets, the technology lends itself to the development of complementary minimally invasive electro-lens probes for directed deep tissue targeting of DNA/RNA delivery.

## 4. Experimental Section

*Guinea Pig Cochlear CC-GET*: The guinea-pig model was used to establish in vivo validation of gene expression using the antibiotic-free pFAR4 gene vector, including establishing duration of expression in the targeted cochlear scala tympani mesenchymal cells and levels of recombinant neurotrophins (BDNF and NT3). All guinea pig experiments were conducted following protocols approved by the UNSW Sydney Animal Care and Ethics Committee (ACEC #: 13/79B; 15/09B; 16/172A), under the Australian National Health and Medical Research Council (NHMRC) guidelines for the care and use of animals for scientific purposes.[63] Guinea pig cochlea CC-GET was undertaken as previously described.[11,15] Young adult guinea pigs of both sexes were anesthetized using isoflurane, and analgesia was provided (buprenorphine (15 µg $kg^{-1}$ i.m., Temgesic, Reckitt Benckiser) and medetomidine hydrochloride (175 µg $kg^{-1}$ i.m., Domitor,

Pfizer Animal Health)) in addition to lignocaine HCl (1% solution; Troy Laboratories), for local pain relief. An incision was made above the mastoid process and a hole was drilled to expose the round window of the cochlea. The CC-GET device developed for clinical application (manufactured by Cochlear Ltd.) was preloaded with pFAR4 DNA resuspended in 10% sucrose, 0.5 mM NaOH at 2 ug $\mu L^{-1}$. This bionic array-derived device was modified from a CI622 type half-banded 22-electrode array configured for dual eight-electrode electric field zones (e22–e15; e14 –7 in "tandem ganged configuration"; after[11]) and incorporated a microfluidics channel for delivery of the plasmid DNA via the tip of the array. The most distal eight electrodes were inserted into the basal turn of scala tympani through a perforation made in the round window membrane and 50 µL was infused over 5 min into the left cochleae only, delivered via a syringe pump. Immediately after DNA infusion the electrical pulse train (10 × 100 µs × 50 mA square wave pulses; 400 µs interpulse interval) was delivered to the clinical CC-GET array via an isolated stimulator (Digitimer DS5) using a custom-built waveform controller and monitoring software which captured the voltage required to deliver each current pulse (enabling measurement of the close-field resistance/conductivity-clamping in the tissue). Experiments that utilized the pFAR4-eGFP plasmid were conducted in normal-hearing animals. Experiments that used the pFAR4-CMVp-BDNF-NT3 plasmid were conducted in guinea pigs that had been deafened using a combination of intravenous furosemide and subcutaneous kanamycin as previously described.[11,15] Details of guinea pig tissue collection and analysis can be found in the Supporting Information.

*Auditory Nerve Regeneration in the Cat*: The neonatal deafened cat model was used for long-term studies evaluating the utility of CC-GET electrotransfer of the clinical neurotrophin encoding DNA for cochlear auditory nerve regeneration and retention with chronic electrical stimulation via CIs. All cat experiments were conducted following protocols approved by the Bionics Institute Animal Research and Ethics Committee and care and practice followed the NHMRC guidelines.[63] Neonatal cats were deafened via daily subcutaneous injections of neomycin trisulphate (60 mg $kg^{-1}$) over 3 weeks from birth, which was confirmed by auditory brainstem response recordings as previously described.[40] Details of the cat CI surgery and pFAR4-CMVp-BDNF-NT3 CC-GET procedure and recording of inferior colliculus multi-channel field recordings mapping cochleotopy, driven by either the neurotrophin gene therapy CI array or the contralateral control array, are described in the Supporting Information.

*CC-GET Targeted DNA Delivery Within the Guinea Pig Brain*: The utility of CC-GET for targeted gene expression in the brain, including proof of concept for neuromodulation, was evaluated in vivo in the guinea pig. All guinea pig experiments were conducted following protocols approved by the UNSW Sydney Animal Care and Ethics Committee (ACEC #: 16/172A) and NHMRC guidelines as above. Animals were anesthetized as described for the guinea pig cochlea CC-GET experiments. Guinea pigs were placed on a heated mat in a small animal stereotaxic frame (model 940, Kopf Instruments), and the scalp was shaved and cleaned with iodine and ethanol wipes. An incision was made through the skin down the midline of the head on top of the skull and retractors were used to keep the incision open. Burr holes were drilled through the skull above the target region. The dura was punctured with a 29 G needle and the CC-GET array was inserted to a depth of 5 mm. The DNA solution was delivered through the array via a syringe microperfusion pump (IM-1, Narashige). Plasmid DNAs: pFAR4-CMVp-eGFP, pJL-hSYNp-ReaChR-tdTomato, pAG-CMVp-GCaMP5g, or pMK-CAGp-eGFP were delivered in 10% sucrose containing 0.5 mM NaOH at a total concentration of 2 µg µL, 1 µg µL each plasmid where cocktails of two plasmids were used. Following the infusion of DNA, pulse trains were delivered to the CC-GET array as described for the guinea pig and cat cochlea experiments. Pulse amplitude was set to either 10, 25, or 50 mA, using either 3 × 100 ms or 10 × 100 µs pulses (see Table S3, Supporting Information). For optogenetic neuromodulation-based $Ca^{2+}$ imaging, three days post CC-GET the brain was extracted immediately following euthanasia, placed into ice-cold sucrose-modified artificial cerebral spinal fluid and cut into 300 µm sections using a vibratome (VT1200S, Leica). Brain slices were imaged on a confocal microscope (LSM710, Zeiss) with ReaChR channelrhodopsin activation evoked using a 561 nm DPSS laser and GCaMP5g $Ca^{2+}$ dynamics detected using 488 nm argon ion laser excitation. For GFP and tdTomato reporter readouts, animals were systemically perfused with phosphate-buffered 4% paraformaldehyde prior to tissue collection, and slices were imaged using the same Zeiss microscope with 488 nm excitation for GFP and 561 nm excitation of tdTomato.

*Statistical Analysis*: Statistical significance was determined using alpha value = 0.05; no data were excluded as outliers (evaluated using the Grubb's test (ESD, extreme studentized deviate; PRISM)). Average data values are reported as mean ± standard error of the mean (s.e.m.), with experimental numbers reported. Statistical analysis was conducted, and graphs were generated using SigmaPlot statistical analysis software (Systat Software Inc. V.14). Parametric statistical assessments were applied following confirmation of normal distribution and equal variance (*t*-tests (single sample, paired and unpaired; one and two-tailed) and one way and two-way ANOVA, including repeated measures where relevant). Data that failed the normal distribution and equal variance tests were transformed and analyzed using nonparametric ranked comparisons (one-way ANOVA on ranks). Post hoc comparisons on ANOVA used the Holm–Sidak method.

## Supporting Information

Supporting Information is available from the Wiley Online Library or from the author.

## Acknowledgements

Ella Trang is thanked for her contributions to supporting the cat auditory nerve regeneration study. Freddy Dueck from Cochlear Ltd is thanked for his support in the development of the clinical CC-GET gene delivery array. Lily Pearson is thanked for her assistance with cell culture imaging. Australian Research Council (ARC) Grants: LP0992098 (GH; Cochlear Ltd. Industry Partner–JFP); LP140101008 (G.H., N.L., M.K., Cochlear Ltd. Industry Partner – PC), and DP151014754 (G.H., N.L., M.K.). National Health & Medical Research Council (NHMRC) grants APP1048764 (M.K., G.H.), APP1189113 (G.H., J.L.P., G.J., M.K., N.L.), APP1091646 (G.H., R.S., N.L., M.K., C.Mc., C.S.B., A.W., J.F., Cochlear Ltd. Partner – J.F.P., P.C., Y.L.E.), APP2013285 (G.H., N.L., M.K., A.A., G.J., J.L.P., D.S.). Passe & Williams Foundation supplementary (G.H., R.S., N.L., M.K., C.Mc., C.S.B., A.W., J.F.) and conjoint grant (G.H., C.S.B., W.L., J.L.P., D.Mc.) funding schemes. Supplementary funding from UNSW Sydney, Macquarie University, NextSense, and NHMRC development grant–linked funding and in-kind support from Cochlear Ltd. as an Industry Partner.

Open access publishing facilitated by University of New South Wales, as part of the Wiley - University of New South Wales agreement via the Council of Australian University Librarians.

## Conflict of Interest

The authors declare no conflict of interest.

## Author Contributions

G.H., J.L.P., N.L., M.K., R.S., C.S.B., C.Mc., A.W., J.F., and J.F.P. performed conceptualization. G.H., J.L.P., N.L., E.C., J.F., A.W., R.S., Y.L.E., P.C., A.A., M.K., C.J.B., J.M.P., J.L., R.G., D.S., and C.M. performed methodology. J.L.P., G.H., E.C., C.J.B., D.H., G.J., A.A., J.M.P., A.W., J.F., Y.L.E., P.C., D.S., and C.M. performed investigation. J.L.P., G.H., A.A., C.J.B., G.J., and E.C. performed visualization. G.H., N.L., M.K., J.L.P., G.J., R.S., C.Mc., C.S.B., A.W., J.F., Y.L.E., P.C., J.F.P., A.A., W.L., D.Mc., and D.S. performed funding acquisition. G.H. and J.L.P. performed project administration. G.H. performed supervision. J.L.P., G.H., and G.J. wrote original draft. J.L.P., G.H., G.J., C.J.B., N.L., A.A., M.K., E.C., D.H., A.W., J.F., R.S., C.S.B., D.Mc., C.Mc., J.M.P., W.L., J.L., R.G., Y.L.E., P.C., J.F.P., D.S., and C.M. wrote, reviewed, and edited.

## Data Availability Statement

The data that support the findings of this study are available in the supplementary material of this article.

## Keywords

CNS electrotransfer, CNS neuromodulation, nerve regeneration, nonviral gene augmentation therapy, precision gene delivery

Received: February 6, 2024
Revised: May 20, 2024
Published online: June 14, 2024

[1] L. Rittié, T. Athanasopoulos, M. Calero-Garcia, M. L. Davies, D. J. Dow, S. J. Howe, A. Morrison, I. Ricciardelli, A. Saudemont, L. Jespers, T. M. Clay, *Mol. Ther.* **2019**, *27*, 1706.
[2] J. A. Kulkarni, D. Witzigmann, S. B. Thomson, S. Chen, B. R. Leavitt, P. R. Cullis, R. van der Meel, *Nat. Nanotechnol.* **2021**, *16*, 630.
[3] C. Sheridan, *Nat. Biotechnol.* **2023**, *41*, 737.
[4] M. P. Rols, in *Springer Protocols: Methods in Molecular Biology*, Humana Press, Totowa, NJ **2008**, *432*.
[5] C. Rosazza, H. Deschout, A. Buntz, K. Braeckmans, M. P. Rols, A. Zumbusch, *Mol. Ther. Nucleic Acids.* **2016**, *5*, e286.
[6] J. M. Escoffre, T. Portet, C. Favard, J. Teissie, D. S. Dean, M. P. Rols, *Biochim. Biophys. Acta.* **2011**, *1808*, 1538.
[7] S. Satkauskas, P. Ruzgys, M. S. Venslauskas, *Expert Opin. Biol. Ther.* **2012**, *12*, 275.
[8] B. Geboers, H. J. Scheffer, P. M. Graybill, A. H. Ruarus, S. Nieuwenhuizen, R. S. Puijk, P. M. van den Tol, R. V. Davalos, B. Rubinsky, T. D. de Gruijl, D. Miklavcic, M. R. Meijerink, *Radiology.* **2020**, *295*, 254.
[9] D. Miklavčič, B. Mali, B. Kros, R. Heller, *Biomed. Eng. Online.* **2014**, *13*, 29.
[10] I. Lacković, R. Magjarević, D. Miklavćić, *IEEE Transact. Dielectr. Electr. Insulat.* **2009**, *16*, 1338.
[11] J. L. Pinyon, S. F. Tadros, K. E. Froud, A. C. Y. Wong, I. T. Tompson, E. N. Crawford, M. Ko, R. Morris, M. Klugmann, G. D. Housley, *Sci. Transl. Med.* **2014**, *6*, 233ra54.
[12] C. J. Browne, J. L. Pinyon, D. M. Housley, E. N. Crawford, N. H. Lovell, M. Klugmann, G. D. Housley, *Gene Ther.* **2016**, *23*, 369.
[13] A. Al Abed, J. L. Pinyon, E. Foster, F. Crous, G. J. Cowin, G. D. Housley, N. H. Lovell, *Front. Neurosci.* **2019**, *13*, 691.
[14] G. D. Housley, C. J. Browne, E. N. Crawford, M. Klugmann, N. H. Lovell, J. L. Pinyon, in *Handbook of Electroporation*, (Ed. D. Miklavčič) Springer, Berlin, Heidelberg **2016**, pp. 1–20.
[15] J. L. Pinyon, G. von Jonquieres, E. N. Crawford, M. Duxbury, A. Al Abed, N. H. Lovell, M. Klugmann, A. K. Wise, J. B. Fallon, R. K. Shepherd, C. S. Birman, W. Lai, D. McAlpine, C. McMahon, P. M. Carter, Y. L. Enke, J. F. Patrick, A. G. M. Schilder, C. Marie, D. Scherman, G. D. Housley, *Hear Res.* **2019**, *380*, 137.
[16] G. D. Housley, N. H. Lovell, J. Pinyon, E. N. Crawford, C. Browne, US 11,213,671 B2, **2022**.
[17] J. L. Pinyon, M. Klugmann, N. H. Lovell, G. D. Housley, *Hum. Gene Ther.* **2019**, *30*, 211.
[18] P. A. Garcia, R. V. Davalos, D. Miklavcic, *PLoS One.* **2014**, *9*, e103083.
[19] S. Hatsushika, R. K. Shepherd, Y. C. Tong, G. M. Clark, S. Funasaka, *Ann. Otol. Rhinol. Laryngol.* **1990**, *99*, 871.
[20] M. Paff, A. Loh, C. Sarica, A. M. Lozano, A. Fasano, *J. Mov. Disord.* **2020**, *13*, 185.
[21] C. Marie, G. Vandermeulen, M. Quiviger, M. Richard, V. Preat, D. Scherman, *J. Gene. Med.* **2010**, *12*, 323.
[22] European_Medicines_Agency, EMEA/CHMP Guideline on the Non-Clinical Studies Required Before First Clinical Use of Gene Therapy Medicinal Products, EMEA/CHMP/GTWP/125459/2006, **2008**.
[23] G. D. Housley, J. Pinyon, N. H. Lovell, A. A. Abed, Method and system for controlling molecular electrotransfer, WIPO–PCT WO 2020/118383 A1, **2020**.
[24] B. C. Thompson, R. T. Richardson, S. E. Moulton, A. J. Evans, S. O'Leary, G. M. Clark, G. G. Wallace, *J. Control Rel.* **2010**, *141*, 161.
[25] P. A. Leake, O. Stakhovskaya, A. Hetherington, S. J. Rebscher, B. Bonham, *J. Assoc. Res. Otolaryngol.* **2013**, *14*, 187.
[26] V. Scheper, I. Seidel-Effenberg, T. Lenarz, T. Stover, G. Paasche, *Brain Sci.* **2020**, *10*, 559.
[27] R. K. Shepherd, A. Coco, S. B. Epp, *Hear Res.* **2008**, *242*, 100.
[28] K. E. Broderick, L. M. Humeau, *Expert Rev. Vaccines.* **2015**, *14*, 195.
[29] R. K. Shepherd, P. M. Carter, A. N. Dalrymple, Y. L. Enke, A. K. Wise, T. Nguyen, J. Firth, A. Thompson, J. B. Fallon, *J. Neural Eng.* **2021**, *18*, 036021.
[30] Australia & New Zealand Clinical Trials Registry (ANZCTR), A phase I/II non-randomized, controlled trial, evaluating the safety and efficacy of neurotrophin gene therapy delivered during cochlear implant surgery, ref. ACTRN12618001556235, http://www.anzctr.org.au/Trial/Registration/TrialReview.aspx?ACTRN=12618001556235 (accessed: June 2018).
[31] Y. Li, Y.-C. Jia, K. Cui, N. Li, Z.-Y. Zheng, Y.-Z. Wang, X.-B. Yuan, *Nature.* **2005**, *434*, 894.
[32] S. F. Tadros, Y. Kim, P. A. Phan, L. Birnbaumer, G. D. Housley, *Histochem. Cell Biol.* **2010**, *133*, 137.
[33] J. Schulze, H. Staecker, D. Wedekind, T. Lenarz, A. Warnecke, *Hear. Res.* **2022**, *413*, 108098.
[34] G. Wan, M. E. Gomez-Casati, A. R. Gigliello, M. C. Liberman, G. Corfas, *Elife.* **2014**, *3*, e03564.
[35] H. Chen, Y. Xing, L. Xia, Z. Chen, S. Yin, J. Wang, *Gene Ther.* **2018**, *25*, 251.
[36] T. G. Landry, J. B. Fallon, A. K. Wise, R. K. Shepherd, *J. Comp. Neurol.* **2013**, *521*, 2818.
[37] A. K. Wise, R. Richardson, J. Hardman, G. Clark, S. O'Leary, *J. Comp. Neurol.* **2005**, *487*, 147.
[38] A. K. Wise, C. R. Hume, B. O. Flynn, Y. S. Jeelall, C. L. Suhr, B. E. Sgro, S. J. O'Leary, R. K. Shepherd, R. T. Richardson, *Mol. Ther.* **2010**, *18*, 1111.
[39] J. B. Fallon, D. R. Irvine, R. K. Shepherd, *Hear. Res.* **2008**, *238*, 110.
[40] J. B. Fallon, D. R. Irvine, R. K. Shepherd, *J. Comp. Neurol.* **2009**, *512*, 101.
[41] C. M. Moore, M. Vollmer, P. A. Leake, R. L. Snyder, S. J. Rebscher, *Hear. Res.* **2002**, *164*, 82.
[42] C. S. Birman, H. Sanli, *Otol. Neurotol.* **2020**, *41*, e458.
[43] B. E. Deverman, B. M. Ravina, K. S. Bankiewicz, S. M. Paul, D. W. Y. Sah, *Nat. Rev. Drug Discov.* **2018**, *17*, 641.
[44] S. Ingusci, G. Verlengia, M. Soukupova, S. Zucchini, M. Simonato, *Front. Pharmacol.* **2019**, *10*, 724.
[45] USA Clinical Trials Registry, Phase I/IIa, First-in-human, Open-label, Single-site Trial of In-vivo Lentiviral Engineered Potassium (K+) Channel (EKC) Gene Therapy for Refractory Epilepsy, https://clinicaltrials.gov/ct2/show/NCT04601974 (accessed: February 2024).
[46] A. D. Van Laar, V. S. Van Laar, W. San Sebastian, A. Merola, J. B. Elder, R. R. Lonser, K. S. Bankiewicz, *J. Parkinsons Dis.* **2021**, *11*, S173.
[47] N. Ohmura, K. Kawasaki, T. Satoh, Y. Hata, *Brain Struct. Funct.* **2015**, *220*, 1307.
[48] H. Wang, C. H. Ko, M. M. Koletar, M. R. Ralph, J. Yeomans, *Eur. J. Neurosci.* **2007**, *25*, 3359.
[49] J. Fan, X. Wu, Z. Cao, S. Chen, C. Owyang, Y. Li, *Gastroenterology.* **2009**, *136*, 1732e3.

[50] F. Wei, X.-M. Xia, J. Tang, H. Ao, S. Ko, J. Liauw, C.-S. Qiu, M. Zhuo, *J. Neurosci.* **2003**, *23*, 8402.
[51] J. D.e Vry, P. Martínez-Martínez, M. Losen, G. H. Bode, Y. Temel, T. Steckler, H. W.m Steinbusch, M. D. Baets, J. Prickaerts, *Mol. Ther.* **2010**, *18*, 1183.
[52] C. J. Hartmann, S. Fliegen, S. J. Groiss, L. Wojtecki, A. Schnitzler, *Ther. Adv. Neurol. Disord.* **2019**, *12*, 175628641983809.
[53] Medtronic, Medtronic 2017 Deep Brain Stimulation Systems doc. UC20190844EN, https://device.report/m/cfb67e9b1a95df6be3816a2b095f792bb471f83a06d398f343cdb581575e2037.pdf (accessed: November 2023).
[54] C. Wrobel, A. Dieter, A. Huet, D. Keppeler, C. J. Duque-Afonso, C. Vogl, G. Hoch, M. Jeschke, T. Moser, *Sci. Transl. Med.* **2018**, *10*, eaao0540.
[55] E. A. Ajay, E. P. Trang, A. C. Thompson, A. K. Wise, D. B. Grayden, J. B. Fallon, R. T. Richardson, *J. Neural Eng.* **2023**, *20*, 026035.
[56] Y. Qiu, N. O'Neill, B. Maffei, C. Zourray, A. Almacellas-Barbanoj, J. C. Carpenter, S. P. Jones, M. Leite, T. J. Turner, F. C. Moreira, A. Snowball, T. Shekh-Ahmad, V. Magloire, S. Barral, M. A. Kurian, M. C. Walker, S. Schorge, D. M. Kullmann, G. Lignani, *Science.* **2022**, *378*, 523.
[57] A. Snowball, E. Chabrol, R. C. Wykes, T. Shekh-Ahmad, J. H. Cornford, A. Lieb, M. P. Hughes, G. Massaro, A. A. Rahim, K. S. Hashemi, D. M. Kullmann, M. C. Walker, S. Schorge, *J. Neurosci.* **2019**, *39*, 3159.
[58] A. J. Craig, G. D. Housley, *Front. Mol. Neurosci.* **2016**, *9*, 34.
[59] L. Yshii, E. Pasciuto, P. Bielefeld, L. Mascali, P. Lemaitre, M. Marino, J. Dooley, L. Kouser, S. Verschoren, V. Lagou, H. Kemps, P. Gervois, A. de Boer, O. T. Burton, J. Wahis, J. Verhaert, S. H. K. Tareen, C. P. Roca, K. Singh, C. E. Whyte, A. Kerstens, Z. Callaerts-Vegh, S. Poovathingal, T. Prezzemolo, K. Wierda, A. Dashwood, J. Xie, E. Van Wonterghem, E. Creemers, M. Aloulou, et al., *Nat. Immunol.* **2022**, *23*, 878.
[60] P. Lemaitre, S. H. Tareen, E. Pasciuto, L. Mascali, A. Martirosyan, Z. Callaerts-Vegh, S. Poovathingal, J. Dooley, M. G. Holt, L. Yshii, A. Liston, *EMBO Mol. Med.* **2023**, *15*, 16805.
[61] X. Xu, W. Chen, W. Zhu, J. Chen, B. Ma, J. Ding, Z. Wang, Y. Li, Y. Wang, X. Zhang, *Cancer Cell Int.* **2021**, *21*, 76.
[62] A. F. Aldoghachi, A. F. Aldoghachi, K. Breyne, K. H. Ling, P. S. Cheah, *Neuroscience.* **2022**, *491*, 240.
[63] NHMRC, *Australian Code for the Care and Use of Animals For Scientific Purposes*, 8th ed., Australian Federal Government National Health and Medical Research Council, Australia **2013**.

ADVANCED SCIENCE
Open Access

# Supporting Information

for *Adv. Sci.*, DOI 10.1002/advs.202401392

Gene Electrotransfer via Conductivity-Clamped Electric Field Focusing Pivots Sensori-Motor DNA Therapeutics: "A Spoonful of Sugar Helps the Medicine Go Down"

*Jeremy L. Pinyon, Georg von Jonquieres, Edward N. Crawford, Amr Al Abed, John M. Power, Matthias Klugmann, Cherylea J. Browne, David M. Housley, Andrew K. Wise, James B. Fallon, Robert K. Shepherd, John Y. Lin, Catherine McMahon, David McAlpine, Catherine S. Birman, Waikong Lai, Ya Lang Enke, Paul M. Carter, James F. Patrick, Robert D. Gay, Corinne Marie, Daniel Scherman, Nigel H. Lovell and Gary D. Housley**

**Advanced Science** Pinyon *et al*., Supporting Information (doi 10.1002/advs.202401392)

# Supporting Information

## GENE ELECTROTRANSFER VIA CONDUCTIVITY-CLAMPED ELECTRIC FIELD FOCUSING PIVOTS SENSORI-MOTOR DNA THERAPEUTICS; '*A SPOONFUL OF SUGAR HELPS THE MEDICINE GO DOWN*'

Jeremy L. Pinyon[1,2], Georg von Jonquieres[1], Edward N. Crawford[1], Amr Al Abed[1], John M. Power[1], Matthias Klugmann[1], Cherylea J. Browne[1,3], David M. Housley[1], Andrew K. Wise[4], James B. Fallon[4], Robert K. Shepherd[4], John Y. Lin[5], Catherine McMahon[6], David McAlpine[6], Catherine S. Birman[6,7,8,9], Waikong Lai[9], Ya Lang Enke[10], Paul M. Carter[10], James F. Patrick[10], Robert D. Gay[10], Corinne Marie[11,12], Daniel Scherman[11,13], Nigel H. Lovell[1] and Gary D. Housley[1*]

**Affiliations:**
[1]Translational Neuroscience Facility, Department of Physiology, School of Biomedical Sciences, Graduate School of Biomedical Engineering, Tyree Institute for Health Engineering (IHealthE), UNSW Sydney, NSW 2052, Australia
[2]Charles Perkins Centre, School of Medical Sciences, Faculty of Medicine and Health, University of Sydney, NSW 2006, Australia
[3]Medical Sciences, School of Science, Western Sydney University, NSW 2560, Australia
[4]Bionics Institute, St Vincent's Hospital, Melbourne, Australia; Department of Medical Bionics; Department of Otolaryngology University of Melbourne, Melbourne 3002, Australia
[5]Tasmanian School of Medicine, University of Tasmania, Hobart, TAS 7001, Australia
[6]Faculty of Medicine and Health Sciences, The Hearing Hub, Macquarie University, Sydney 2109, Australia
[7]Faculty of Medicine and Health, University of Sydney, Sydney, NSW 2006, Australia
[8]Department of Otolaryngology, Royal Prince Alfred Hospital, Camperdown, NSW 2050, Australia
[9]NextSense, Royal Institute of Deaf and Blind Children, Gladesville, NSW 2111, Australia
[10]Cochlear Limited, 1 University Avenue, Macquarie University, NSW 2109, Australia
[11]Université Paris Cité, CNRS, Inserm, UTCBS, F-75006 Paris, France
[12]Chimie ParisTech, Université PSL, 75005 Paris, France
[13]Fondation Maladies Rares, 96 rue Didot, 75014 Paris, France

Corresponding Author*
Gary D. Housley
School of Biomedical Sciences
Faculty of Medicine & Health
UNSW Sydney
NSW 2052
Australia
E: g.housley@unsw.edu.au
T: +61404235180

# Supporting Information Content Summary

**Tables**



**Primary figure commentary** (Figs. 1, 2, 4, 6 and 7)

## Supporting Information - Materials and Methods

### Electric Field Recordings

To establish the effect of conductivity - clamping on the GET electric field, voltage potentials were measured adjacent to the GET array (modified from an 8 electrode research cochlear implant (CI) array, Cochlear Limited, Australia, part number Z60274) (after [1]). This was done in either non-conductive (10% sucrose), or conductive (0.9% sodium chloride) solutions, with or without 2 mg/ml salmon sperm DNA sheared to an average length of 2.0 kb (Merk). The GET array electrodes were driven in the 'tandem' configuration, with four ganged anodes and four ganged cathodes, as shown in Figure 1A, using either a DS5 isolated stimulator (Digitimer) for fixed recording electrode position experiments (Figure 1A, B), or an A-M Systems 2200 stimulus isolator for field mapping (Figure 1C, D) to drive 100 ms square wave pulses. Pulses were controlled and voltage and current outputs monitored (five channels at 100 kHz sampling rate) using a Digidata 1440 interface (Axon Instruments) with Clampex software (version 10.2.0.12; Axon Instruments). A custom-built electrode monitoring system was used to provide independent measurements of voltage in the field, and both voltage and current applied at the electrodes. The recording electrode was a custom platinum fine tip electrode, referenced to a platinum ground electrode positioned distal to the GET array and the generated electric field. Measurements were taken at ~ 95 ms during the 100 ms pulses. Electrodes were positioned using a translational stage (SliceScope Pro 6000; Scientifica, East Sussex, UK) and micromanipulator (ROE-200; Sutter Instrument Company, Novato, CA, USA) with 0.5 mm resolution steps.

### HEK293 cell monolayer modelling

The HEK293 cell monolayer was used as a high-throughput *in vitro* model to establish a reporter-based biomarker of the suprathreshold electric field for GET. Adherent HEK293 cells were maintained and prepared for transfection experiments by seeding onto 18 mm round glass coverslips ~ 24 hr prior to transfection, which was undertaken at ~50% cell confluence, following protocols previously published ([1-3]). Plasmid DNA resuspended at 2 mg/ml was delivered to the HEK293-coated coverslips in 20-30 µl of 10% sucrose, with or without 0.5 mM NaOH, or saline, with or without 50 mM Tris buffer, or 9% sucrose + 0.09% NaCl + 0.5 mM NaOH. Electric pulse trains were delivered via a DS5 (Digitimer) isolated stimulator using a custom-built waveform control and monitoring software. Transfected coverslips were imaged

2-4 days after GET on a LSM710 confocal microscope (Zeiss) using a 488 nm argon ion laser for GFP and a 561 nm DPSS laser for mCherry. For larger fields of transfection, multiple overlapping tiled images were captured and assembled prior to analysis. Boundaries around the region of transfected cells were delineated and the area of transfection or total fluorescence (sum pixel intensity) calculated using ImageJ (US NIH).

**Cochlear implant surgery and pFAR4-BDNF-NT3 CC-GET in cats**

At ~ 3 months of age, cats underwent CC-GET prior to bilateral implantation of a HL14 CI electrode array (Cochlear Ltd.). The surgery was performed as previously described [4] with the exception that prior to implantation of each cochlea CC-GET was undertaken using a double-insertion technique where the clinical CC-GET array was inserted, GET performed and the CC-GET array was removed prior to insertion of the permanent HL14 array for chronic stimulation as a 'bionic ear' hearing prosthesis. CC-GET was undertaken as described for the guinea pig experiments above, but performed bilaterally with randomization of cochlea receiving the pFAR4-CMVp-eGFP DNA and the contralateral cochlea receiving the pFAR4-BDNF-NT3 DNA.

Clinical CIs and speech processors were switched on two weeks after implantation and chronic stimulation in response to environmental sound was presented continuously, except for brief periods when batteries were replaced. Standard clinical frequency allocation tables were used to program speech processors for monopolar stimulation. Biphasic pluses were delivered to each electrode at 500 pulses per second and had a 25 μs phase interval with an 8 μs inter-phase gap. Impedance of the intracochlear electrodes was measured weekly throughout the chronic stimulation period using monopolar stimulation from each intracochlear electrode to the external return electrode via Custom Sound EP 2.0 software (Cochlear ltd.).

**Neural response telemetry (NRT) electrocochleography recording of electrically evoked compound action potentials (eCAPS)**

The level of the CI electrodes were recorded for both ears in awake animals every 2-3 weeks throughout the chronic stimulation period using Custom Sound EP 2.0 software (Cochlear ltd.). NRT stimulation pulses were delivered to each of the 14 electrodes in monopolar stimulation using monopolar stimulation (MP+1) to the external reference electrode at 25 μs/phase biphasic pulses delivered at 80 pulses per second. ECAPs were recorded at 10 CL (Current Level) intervals from a maximum of 250 CL to below threshold.

**Terminal inferior colliculus recordings**

Approximately six months after CC-GET and cochlear implantation acute electrophysiological recordings were taken in the inferior colliculus (IC) immediately prior to euthanasia as previously described [5] over a 24-72 hour period. The multi-electrode array IC recording site was driven by each of the CI arrays inserted into control eGFP DNA and neurotrophin DNA – CC-GET treated cochleae. In anesthetized cats 32-channel, 100 μm spacing, recording electrodes on a silicon substrate (NeuroNexus Technologies, USA) were inserted into the IC bilaterally to a depth of ~ 3.5 mm. Anesthesia was induced by intramuscular injection of ketamine (20 mg/kg) and subcutaneous injection of xylazil (2 mg/kg) and maintained by intravenous infusion of sodium pentobarbital (3-8 mg/kg/hr). Spike activity was acquired from the 64 electrodes using a Cerebus acquisition system (Blackrock Microsystems, USA), with sampling of amplified and filtered data at a rate of 30 kHz. Bipolar stimulation delivered to adjacent intracochlear electrodes of the CI array was 100 μs phase duration and 50 μs inter-phase gap, bipolar cathodic-first charge balanced at rate of 4 Hz. This was delivered via an in-house designed multi-channel stimulus generator at CL ranging between 0 and 265 CL (defined by Cochlear Ltd.) where, current in μA = 17.5*(100 ^ (CL/255). Neural activity was detected

based on threshold (4x root-mean-square level) crossings and spikes in a 3 - 45 ms post stimulus window. At each recording site, the spike counts were recorded across 10 trials for each stimulation configuration and current level to calculate spontaneous activity. IC spatial turning curve (STC) width was determined by calculating the average threshold value across the first five electrodes of the 32-electrode IC array for each of the CI electrodes, for each cochlea. The STC width was then defined as the length of the array where electrodes had a threshold value below the average threshold across the first five electrodes.

**Plasmid DNA**

Plasmids maps for each of the seven DNA molecules used are shown in Figure S1. For transfection, plasmids were purified from *E. coli* using Plasmid Maxiprep Kits (Qiagen) according to the instructions. DNA pellets were resuspended in water for quantification on a Nanodrop Nd-1000 spectrophotometer (ThermoFisher). Quantified DNA was dried using a SpeedVac vacuum concentrator (ThermoFisher) at room temperature and resuspended in isotonic saline or sucrose solutions at the desired concentration for transfection.

**Guinea pig tissue collection and analysis**

Guinea pigs were euthanized using intraperitoneal injection of pentabarbitol (100 mg/kg). Cochlea were isolated and fixed by perfusion of the cochleae scala with 4% paraformaldehyde in phosphate buffer and submerged in 4% paraformaldehyde at 4 ºC overnight. Perilymph was collected prior to fixation using a 20 µl pipette placed in the round window after perforation of the round window membrane. Perilymph was placed in 1.5 ml microcentrifuge tubes, snap frozen in liquid nitrogen and stored at -80 ºC for BDNF and NT3 ELISA. Samples from brain, heart, blood, mastoid process muscle, liver, kidney, stool and urine were collected and snap frozen in liquid nitrogen for subsequent PCR analysis. After fixation, cochleae were decalcified at 4 ºC in phosphate buffered 8% EDTA (pH7.6) for 2 weeks. Cochleae from experiments using pFAR4-eGFP were hemi sectioned with a scalpel blade and whole-mount imaged on a LSM710 platform (Zeiss) to quantify the number of GFP transfected cells. Cochleae from deafened guinea pig experiments using pFAR4-CMVp-BDNF-NT3 to assess capacity for auditory neuron regeneration were cryoprotected in 30% sucrose prior to cryosection into 50 µm sections, and immunolabelling free-floating for TUBB3 (β3Tubulin; clone TUJ1 Covance) as previously described (Pinyon 2014, Pinyon 2016). Immunolabelled sections were mounted on coverslips using Prolong Gold mounting media (P36931; ThermoFisher) and imaged on a LSM710 platform with a 488 nm argon ion laser. Images were analyzed for neurite regeneration via fluorescence intensity of the TUBB3-labelled auditory neuron peripheral processes using ImageJ (US NIH). The segmented line tool was used to delineate the distal 50% of the osseus spiral lamina region (corresponding to the most pronounced region of neurite density loss at one month – post deafening. The average pixel intensity in this region was determined for sections from each of the four left (deafened with pFAR4-CMVp-BDNF-NT3 delivery) and the control right (deafened only) cochleae.

**Cat tissue collection and analysis**

Following electrophysiological recordings in the IC, animals were euthanized via intraperitoneal injection of 100 mg/kg pentobarbital and perfused systemically with heparinized 0.9% saline prior to 4% paraformaldehyde at 4 ºC. Cochleae were isolated and fixed for an additional hour submerged in 4% paraformaldehyde at 4 ºC. Cochleae were decalcified in 10% EDTA for 2 weeks then cryoprotected with 30% sucrose before freezing and cryosectioning at 50 µm. Free-floating sections were immunolabelled for TUBB3 (β3Tubulin; clone TUJ1

Covance) and NF200 (neurofilament protein 200 kDa; Cat# N4142, Merck) with respective secondary antibodies goat anti-mouse Alexa Fluor™ 488 (A-11001; ThermoFisher) and goat anti-rabbit Alexa Fluor™ 594 (A-11072; ThermoFisher). All antibodies were used at 1:1000 dilution. Sections were immunolabelled, mounted, imaged and analyzed for neurite regeneration as described above for the guinea pigs, with all sections containing the basal turn osseous spiral lamina (OSL) analyzed (n = between 7 and 10 sections per cochlea, with OSL areas measured between 32,334 and 57,259 square microns. Additionally, average fluorescence intensity of the auditory neuron somata was analyzed in ImageJ (US NIH) using the elliptical selections tool to outline each soma. Four sections from each cochlea were analyzed with between 9 and 61 somata measured from each section. Fluorescence intensity of both cell somata and neurites was measured in the 488 nm argon ion laser channel (TUBB3 immunodetection). At the time of euthanasia additional samples (blood, brain, heart, liver, kidney, lung, spleen, skin, intestine, and muscle from beside the ear canal) were collected and snap frozen in liquid nitrogen for PCR analysis. Samples then underwent DNA extraction and PCR analysis.

**Montecarlo analysis of CC-GET electric field thresholds**

A finite element model was developed to simulate the electric potential within the media surrounding the 8-electrode cochlea array in the *in vitro* HEK293 cell CC-GET model. Model input parameters include the media volume, the height of the media and the meniscus forming over the array (100 μm), the long semi-axis of the ellipse defining the meniscus, the supply voltage (120 V), and the voltage loss across the electrode-electrolyte bilayer, and the conductivity of the media. Experimentally indeterminate parameters were defined using a Monte-Carlo approach and were randomly selected from a uniform distribution to generate a population of models (n = 10), long-axis of the ellipse defining the meniscus (range 0.3-1.3 mm), voltage loss across the bilayer were random (range 2 – 30 V). This produced a media volume of 21-30 μl, approximating that used experimentally. For each model, the media specific conductivity was estimated by a parameter optimization routine that minimized the difference between the experimentally recorded total system resistance (4000 Ohm) and the model predicted total resistance. For each model (n = 10), the electric field threshold was then estimated by identifying a uniform perimeter symmetrically around the array that enclosed an area equal in size to the area of HEK293 cell transfection measured experimentally.

**Measurement of recombinant BDNF and NT3 by ELISA**

BDNF and NT3 levels in HEK293 cell culture supernatant (four days post CC-GET) and in guinea pig perilymph samples (2 weeks post CC-GET) were analyzed. ELISA-based quantification of BDNF (R&D Systems catalogue number DY248) and NT3 (R&D Systems catalogue number DY267) was performed as specified by the manufacturer, followed by colorimetric readout measuring absorbance at 415 nm in a FLUOstar microplate reader (PerkinElmer). BDNF and NT3 concentration was extrapolated against a serial dilution of the relevant purified neurotrophin standard.

**PCR probe for tissue dispersion of neurotrophin miniplasmid**

Samples were thawed and DNA was purified via the HotShot alkaline lysis method [6]. PCR was then performed on the extracted DNA to detect any possible undegraded plasmid DNA still present, using a forward primer located in the codon optimized BDNF coding sequence (5'-GGTTCATCAGGATCGACACTTCC-3') and reverse primer located in the IRES (5'-GGAATGCTCGTCAAGAAGACAGG-3'). PCR was conducted using Taq Polymerase with Thermopol Buffer (New England Biolabs) at 97 ºC for 2 min, followed by 40 cycles of 97 ºC for 30 s, 64 ºC for 30 s and 72 ºC for 1 min with a final elongation of 72 ºC for 5 min.

## Supporting Information – Figures and Tables

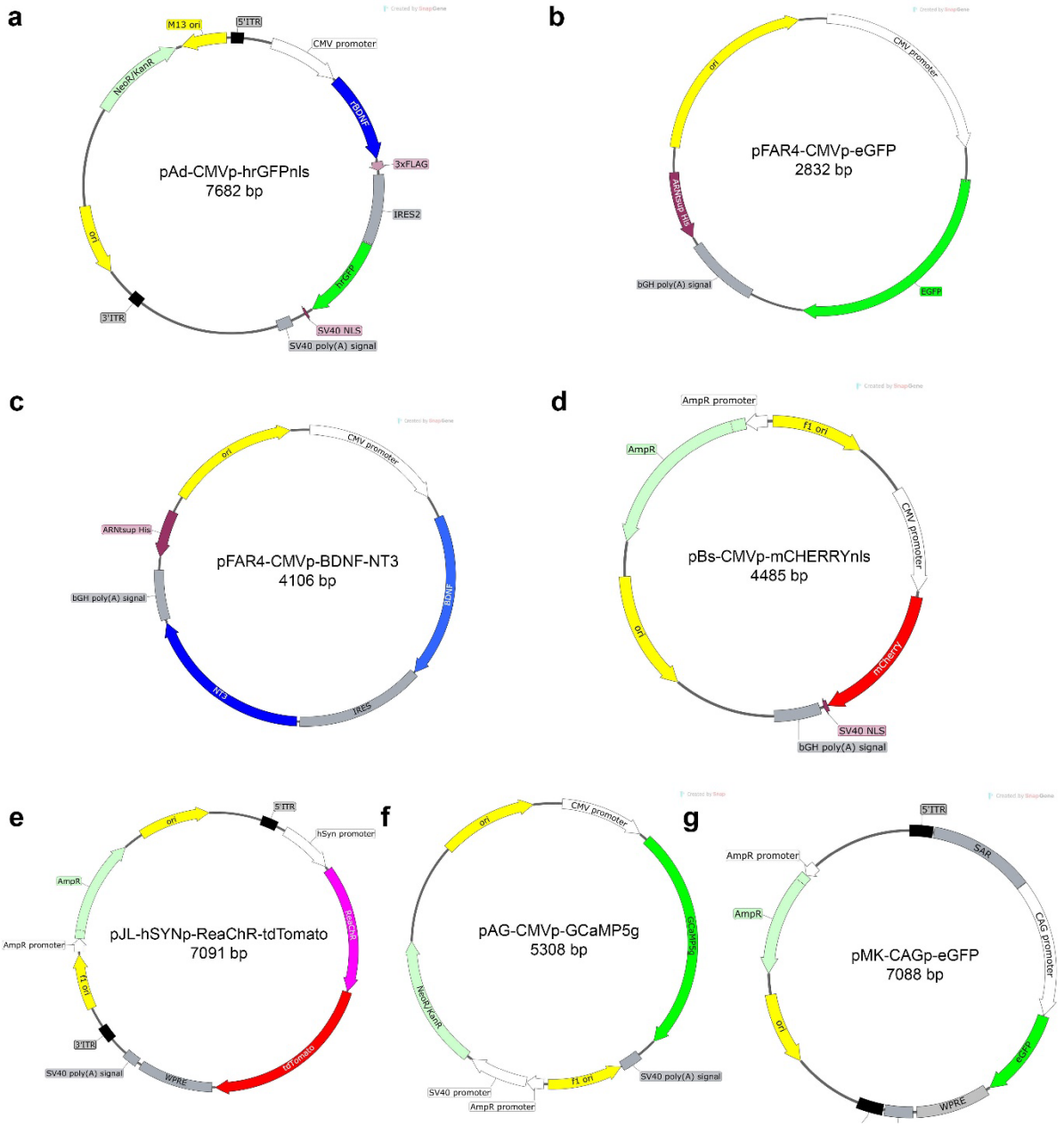


**Figure S1. Plasmid maps showing the design of neurotrophin, reporter, and optogenetic expression vectors**. (**A**) pAd-CMVp-hrGFPnls, used as a reporter plasmid, containing the nuclear localized humanized renilla GFP (hrGFPnls) reporter coding sequence as the second cistron downstream of an internal ribosome entry sequence (IRES) and the rat brain derived neurotrophic factor (rBDNF) coding sequence driven by the cytomegalovirus promoter (CMVp). (**B**) pFAR4-CMVp-eGFP, a miniplasmid free of antibiotic resistance genes (pFAR) containing the enhanced GFP (eGFP) coding sequence. The pFAR4 plasmid vector enables production of plasmids lacking the conventional antibiotic resistance selection marker genes, pFAR4 plasmids are produced using a genetically modified *E. coli* strain that contains a nonsense mutation in the essential thymidylate synthase (*thyA*) gene generating its thymidine

auxotrophy. pFAR4 plasmids encode a nonsense suppressor t-RNA that restores the ThyA open reading frame and bacterial growth, thus avoiding the use of antibiotic resistance marker for selecting plasmid-containing bacteria. These plasmids are compatible with clinical translation under EMA guidelines for gene electrotransfer, as they lack antibiotic resistance genes, thereby preventing inadvertent conferral of antibiotic resistance in commensal bacterial in the surgical field (after [7]). (**C**) pFAR4-CMVp-BDNF-NT3 contains the same miniplasmid backbone as (B) but with human BDNF and neurotrophin-3 (NT3) cistrons separated by an IRES. (**D**) pBs-CMVp-mCHERRYnls depicts the reporter plasmid used for the experiments shown in Fig. 4. (**E**) pJL-hSYNp-ReaChR-tdTomato contains a fusion protein of the red-shifter channelrhodopsin (ReaChR) and 2x tdTomato reporter under the control of the human synapsin promoter (hSYNp). (**F**) pAG-CMVp-GCaMP5g depicts the genetically encoded $Ca^{2+}$ reporter. (**G**) pMK-CAGp-eGFP contains the eGFP reporter downstream of the cytomegalovirus-Chicken beta-actin-rabbit beta-globin hybrid synthetic promoter (CAGp).

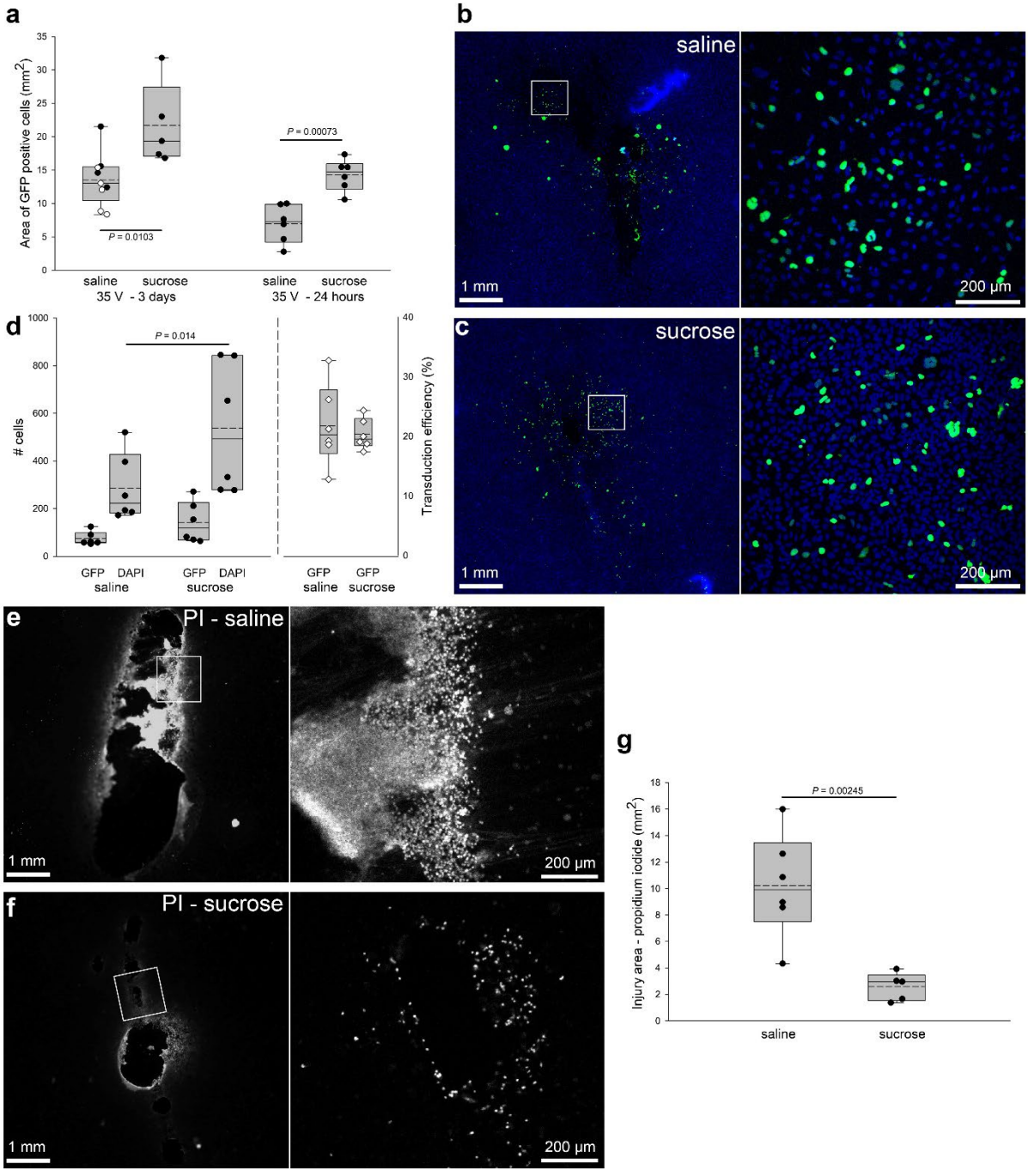


**Figure S2. Increase in area of transfected HEK293 cells expressing GFP following CC-GET at equivalent applied voltage using sucrose DNA carrier solution (conductivity-clamping) compared with saline carrier; efficiency and cell injury prevention. (A)** 3 day cell culture study (left box plot set): 3 x 100 ms pulses at 35 V applied ($V_a$) to the gene electrotransfer (GET) probe. pAd-CMVp-hrGFPnls plasmid (2 µg/µl) in 10% sucrose (black circles), or in normal saline (0.9% NaCl) with (black circles) or saline + Tris Buffer (50 mM, pH7.4; open circles; data for saline experiments were pooled; $P > 0.05$, t-test). The size of fields of the nuclear localized GFP+ve cells within HEK293 cell monolayers after 3 days in culture were determined by drawing boundaries around the perimeter of reconstructed montages of confocal images. Box plots show 25% and 75% boundary layers with 95% limits, lines show

median values, dashed lines are means; data from individual experiments overlaid. Student's t-test. Demonstrating the reduction in charge transfer achieved by CC-GET, only 5 mA was required to achieve 35 $V_a$ using the sucrose carrier, compared with 50 mA current pulses for the same $V_a$ when using saline carrier. Data reflected in US patent ref. [8] Right-side box plots report on a 24 hour cell culture study using the same GET parameters for sucrose vs. saline carriers. This replicated the finding of the 3 day cell culture study where sucrose carrier similarly achieved a larger area of transduced cells. This experiment included DAPI staining post-fixation to enable cell counts of regions of interest (ROI) (**B**,**C**; whole field (Olympus Slideview VS200) images showing ROI, detailed in adjacent confocal LSM images, for saline and sucrose carriers respectively). (**D**) These 24 hour cell culture data indicated an equivalent relative gene expression efficiency using saline and sucrose carriers, against a background of lower cell counts in the saline carrier condition (two way ANOVA with Holm-Sidak post-hoc comparison). (**E**,**F**,**G**) demonstrate the impact of the saline carrier for GET on cell viability using the same GET conditions, with propidium iodide (2 µg/ml) added to the culture medium 1 hour after GET to label cells with irreversible electroporation / injury, followed by PFA fixation and imaging. E and F show whole field and detail confocal LSM images of the region in the vicinity of the gene delivery array placement on the HEK293 cell monolayer in saline and sucrose carrier conditions. (G) PI fluorescence delineating cell injury margin surrounding a mechanical artefact associated with contact of the electrodes with the cell layer (as delineated by the sucrose carrier area measurements, where PI signal is minimal) (t-test).

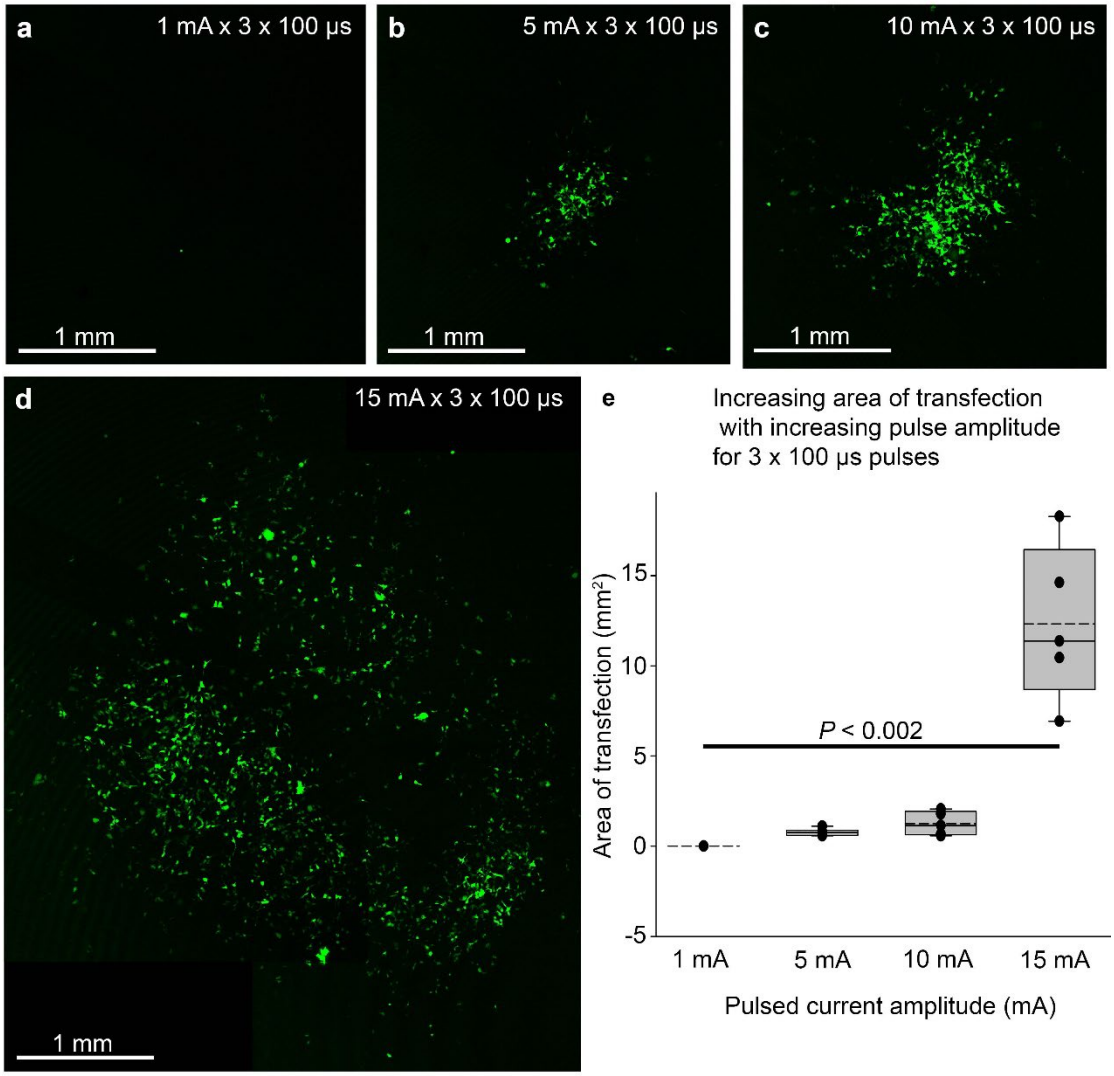


**Figure S3. Determination for threshold for reporter plasmid expression with CC-GET DNA electrotransfer using low conductivity-clamping via application of 10% sucrose DNA carrier solution.** This CC-GET utilized an adapted 5 mm 8 electrode array (Cochlear Ltd.). (**A-D**) Adherent HEK293 cells on coverslips in culture (3 days) demonstrate GFP expression following electrotransfer of reporter plasmid DNA (pAd-CMVp-hrGFPnls plasmid (2 µg/µl)) using 3 x 100 µs square wave current pulses varying between 1 – 15 mA. (**E**) Box plots show 25% and 75% boundaries, with 95% levels as bars, individual data overlaid (n = 5 per group); lines indicate median, dashed lines indicate means. *P* value shown reflects ANOVA on ranks comparing 15 mA with lower current levels. 1 mA produced minimal expression ($P < 0.001$ vs. 5 mA; t-test). Images from US patent ref. [8]

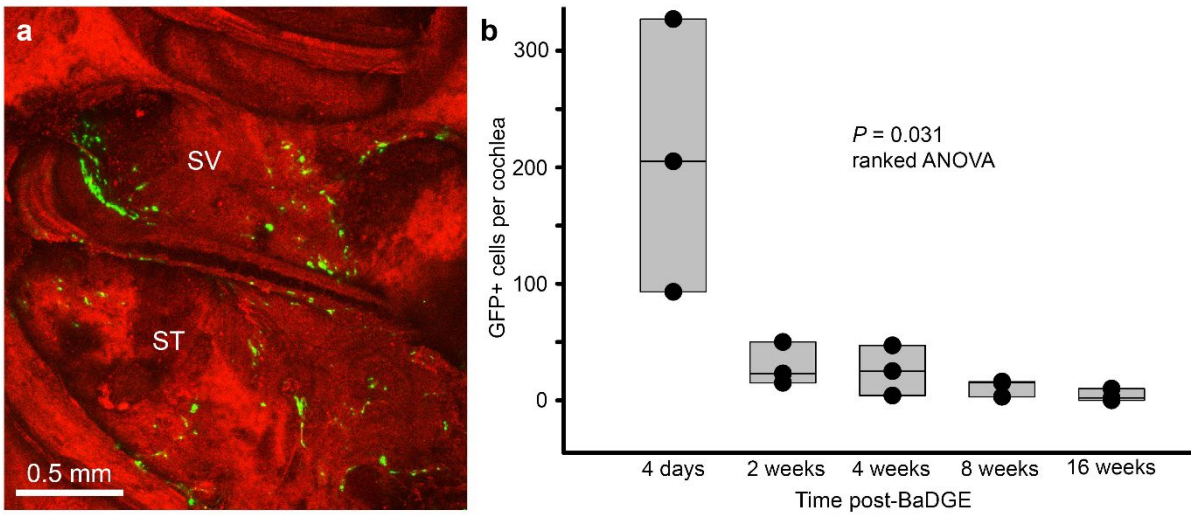


**Figure S4. Longitudinal study of CC-GET - directed expression of the pFAR4-CMVp-eGFP reporter plasmid to the cells lining the guinea pig cochlea basal region perilymphatic scalae.** The cell counts of GFP+ve mesenchymal cells (green) is highest 4 days after gene electrotransfer and under-represents the total due to clustering. Data from 4 days to 16 weeks after *in vivo* delivery to the basal scala tympani chamber demonstrated significant attenuation in expression. pFAR4-CMVp-eGFP miniplasmid delivered using the clinical CC-GET device (10 x 100 µs x 50 mA pulses). (**A**) reconstructed confocal image stack of the scalae of the basal region of the cochlea achieved by removal of the lateral wall. ST, scala tympani; SV scala vestibuli. Red is autofluorescence. (**B**) Box plots of the counts of GFP expressing cells at time points out to four months following CC-GET delivery of the naked GFP-encoding DNA (25% and 75% boundaries, thin line reflects the median; individual data overlay; ANOVA P value reflects time-dependent decline in expression attributable to turn-over of the targeted mesenchymal cells [3]; n = 15).

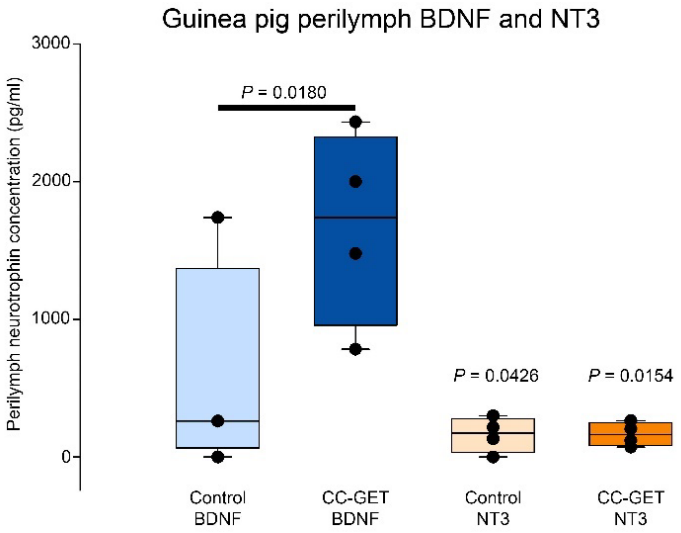


**Figure S5. Cochlear perilymph recombinant neurotrophin levels in deafened guinea pigs two weeks after CC-GET delivery of clinical pFAR4-CMVp-BDNF-NT3 DNA.** BDNF and NT3 ELISA assays (see Supporting Information - methods). Box plots reflect 25% - 75% boundaries with 95% limits. Median = solid line; mean = dashed line, data overlaid; paired Student's t-test analysis for BDNF comparison against the untreated contralateral (control) cochleae; one-tailed single sample t-tests for NT3 data (n = 4).

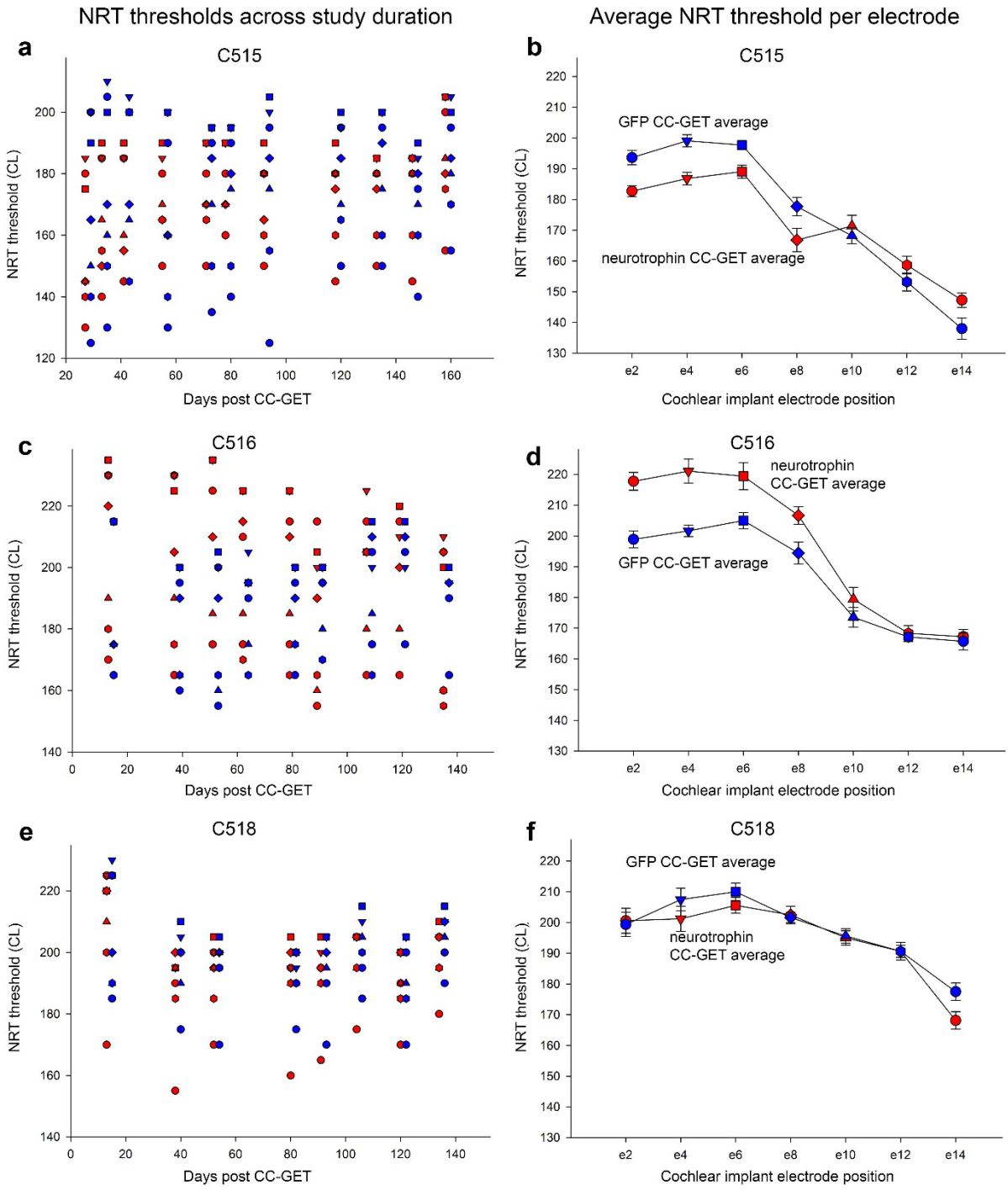


**Figure S6. Electrically evoked compound action potential (ECAP) thresholds after CC-GET delivery of neurotrophin or control (eGFP) DNA to the cochleae of deafened cats, supporting long-term hearing using bilateral cochlear implants.** **(A,C,E),** Electrically - evoked compound action potential thresholds measured via cochlear implant nerve response telemetry with monopolar stimulation (MP+1) over time (cat ID: C515, 159 days; C516, 136 days; C518, 135 days) at electrodes e2, e4, e6, e8, e10, e12 & e14 (shown as different symbols

in each vertical stack) for CC-GET delivery of neurotrophin encoding DNA (red; pFAR4-CMVp-BDNF-NT3), and the control DNA (blue; pFAR4-CMVp-eGFP). These data show that the neural recruitment thresholds along the length of the cochlear implant array were stable over time. This is also evident from the limited variance (s.e.m.) around the mean for each electrode across the study period (**B,D,F**). Note the symbols for each electrode in these Figure elements corresponds to the data for individual electrodes at each test day shown in (A,C,E). There was no significant difference between thresholds at different positions along the cochlear implant arrays attributable to a neurotrophin DNA CC-GET effect ($P = 0.755$), while a pronounced position-dependent effect was evident ($P < 0.001$; two-way ANOVA), where thresholds declined towards the apex (electrode e14) of the cochlear implant array.

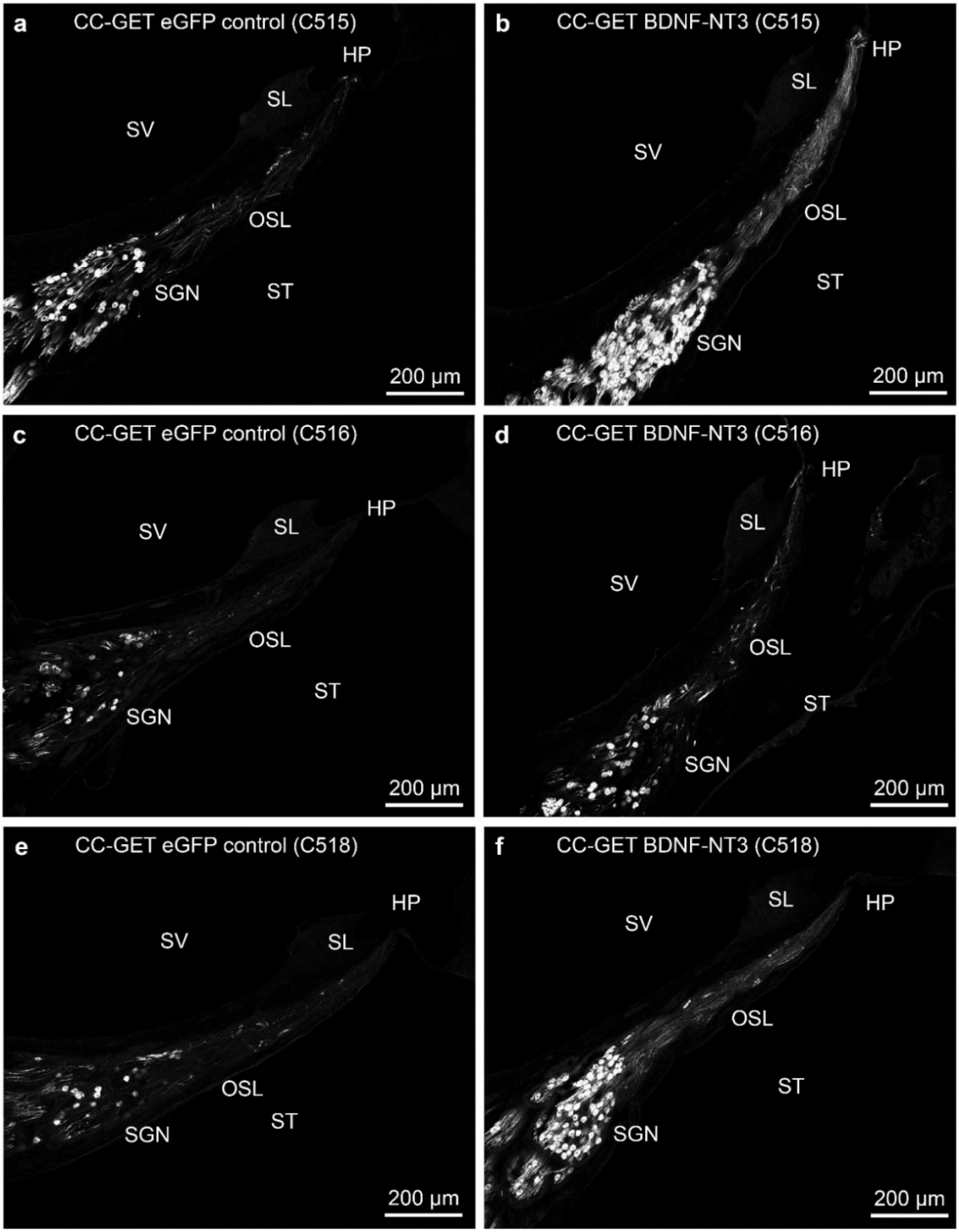


**Figure S7. Sustained regeneration of the peripheral spiral ganglion neurites in the cochleae of deafened cats supported by chronic cochlear implant stimulation following CC-GET delivery of neurotrophin-encoding DNA.** CC-GET delivery of pFAR4-CMVp-BDNF-NT3 DNA (BDNF-NT3) followed by continuous use of a cochlear implant device sustained the regenerated auditory nerve fibers (135 – 159 days post CC-GET). The controls are the opposite cochleae where CC-GET delivered the pFAR4-CMVp-eGFP - encoding DNA (eGFP). TUBB3 (β III tubulin) immunofluorescence demonstrates enhanced neurite labelling in the osseous spiral lamina (OSL) and in the somata of the spiral ganglion neurons (SGN). HP, habenula perforata; SL, spiral limbus; ST, scala tympani; SV, scala vestibuli.

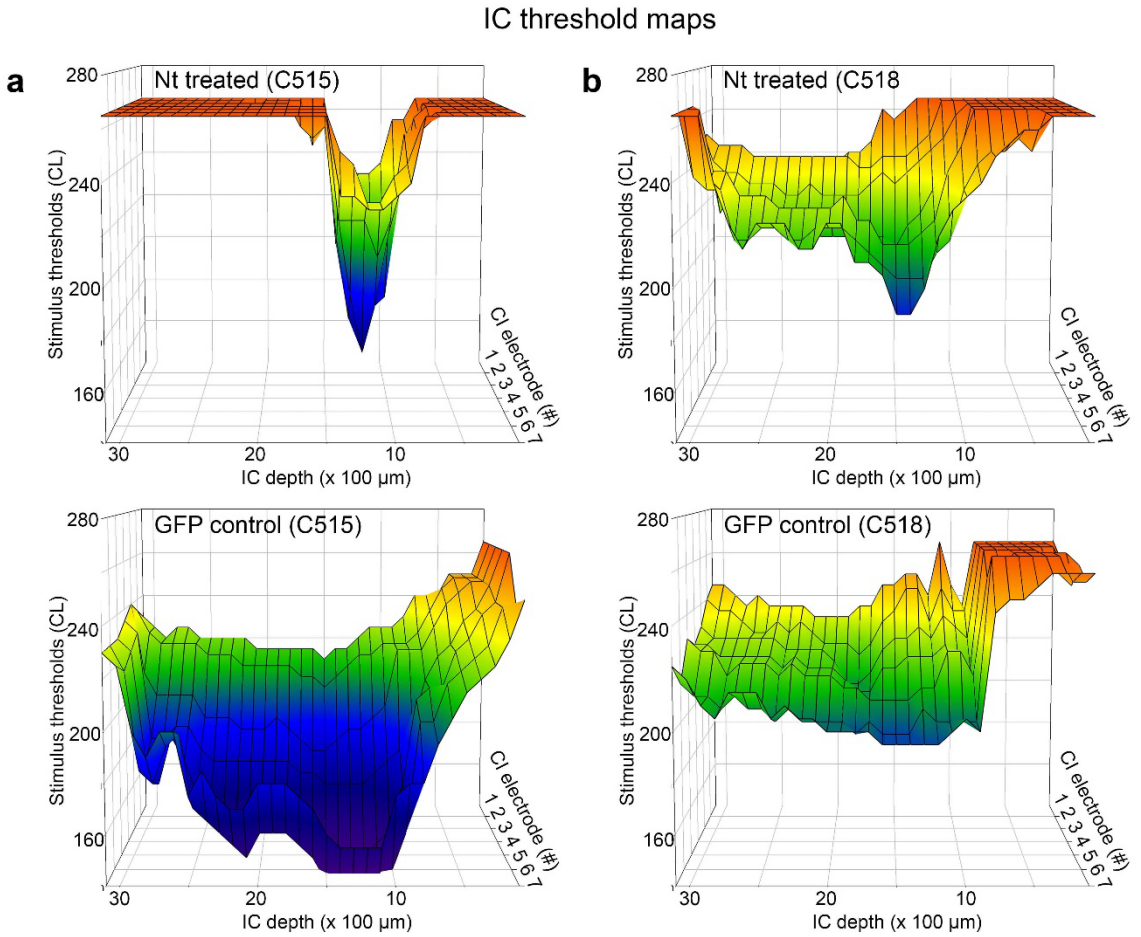


**Figure S8. Sharpening of inferior colliculus spatial tuning curves with cochlear CC-GET delivery of BDNF–NT3 neurotrophin DNA followed by chronic cochlear implant stimulation in the deafened cat.** Data are recorded from the same 32 channel array inserted into the inferior colliculus, with stimulation across seven cochlear implant electrodes for (**A**) each of pFAR4 CMVp-BDNF-NT3 CC-GET - treated cochlea and (**B**) the contralateral (control) pFAR4 CMVp-eGFP CC-GET – treated cochlea. Following the bilateral CC-GET with (neurotrophin (Nt) encoding DNA into one cochlea and control (eGFP) DNA into the opposite cochlea, the cats received bilateral cochlear implants (CI), which were switched on two weeks after the surgery and remained active for the duration of the study (C516, 135 days; C518 136 days). Data from the third cat is shown in Figure 6. Stimulus threshold of the evoked field potentials was determined as bipolar CI stimulus level (CL, current level).

**Table S1. Pulse parameters and resistivity for *in vivo* guinea pig cochlear DNA electrotransfer via the clinical CC-GET device**

| **Plasmid (DNA 2 µg/µl in 10% sucrose carrier)** | **Electrotransfer mean pulse amplitude (mA)*** | **Electrotransfer mean applied voltage (V)** | **Local resistance (kΩ)** | **Animal ID** |
|---|---|---|---|---|
| normal hearing | (50 mA set) | | | |
| pFAR4-CMVp-eGFP | 50 | 70 | 1.40 | #3 |
| pFAR4-CMVp-eGFP | 50 | 70 | 1.40 | #4 |
| pFAR4-CMVp-eGFP | 35 | 120 | 3.43 | #6 |
| pFAR4-CMVp-eGFP | 29 | 120 | 4.14 | #7 |
| pFAR4-CMVp-eGFP | 50 | 106 | 2.12 | #8 |
| pFAR4-CMVp-eGFP | 43 | 118 | 2.74 | #9 |
| pFAR4-CMVp-eGFP | 42 | 116 | 2.76 | #11 |
| pFAR4-CMVp-eGFP | 48 | 116 | 2.42 | #14 |
| pFAR4-CMVp-eGFP | 45 | 114 | 2.51 | #15 |
| pFAR4-CMVp-eGFP | 50 | 92 | 1.80 | #16 |
| pFAR4-CMVp-eGFP | 49 | 114 | 2.32 | #17 |
| pFAR4-CMVp-eGFP | 50 | 85 | 1.70 | #18 |
| Mean ± s.e.m., n | 45.1 ± 1.98 mA | 103.4 ± 5.51 V | 2.40 ± 0.24 | n = 12 |
| | | | | |
| -deafened- | (50 mA set) | | | |
| pFAR4-CMVp-BDNF-NT3 | 38 | 120 | 3.15 | #234 |
| pFAR4-CMVp-BDNF-NT3 | 25 | 120 | 4.90 | #235 |
| pFAR4-CMVp-BDNF-NT3 | 37 | 120 | 3.30 | #236 |
| pFAR4-CMVp-BDNF-NT3 | 23 | 120 | 5.30 | #237 |
| Mean ± s.e.m., n | 30.8 ± 3.92 | 120 ± 0.00 | 4.16 ± 0.55 | n = 4 |
| | | Average across groups | **2.84 ± 0.29** (n = 16) | |

| | | | | |
|---|---|---|---|---|
| Cochlear perilymph reference (baseline) | | | | |
| | - | - | 0.815 | #234 |
| | - | - | 0.657 | #235 |
| | - | - | 0.831 | #236 |
| Mean ± s.e.m., n | | | 0.77 ± 0.06 kΩ | n = 3 |

* gene electrotransfer pulse train 10 x 100 µs at set current level of 50 mA; Current levels below 50 mA reflect rail voltage of current controller (Digitimer DS5 analog-controlled stimulator).

**Table S2. Pulse parameters and resistivity for *in vivo* cat cochlear DNA electrotransfer via the clinical CC-GET device**

| **Plasmid (DNA 2 µg/µl in 10% sucrose carrier)** | **Electrotransfer mean pulse amplitude (mA)** | **Electrotransfer mean applied voltage (V)** | **Local resistance (kΩ)** | **Animal ID** |
|---|---|---|---|---|
| | | | | |
| pFAR4-CMVp-eGFP | 38 (50 set) | 120 | 3.16 | Cat#1 - left |
| pFAR4-CMVp-eGFP | 38 (50 set) | 120 | 3.16 | Cat#1 - right |
| pFAR4-CMVp-eGFP | 23 (40 set) | 120 | 5.22 | C515 - left |
| pFAR4-CMVp-BDNF-NT3 | 34 (40 set) | 120 | 3.53 | C515 - right |
| pFAR4-CMVp-BDNF-NT3 | 35 (40 set) | 120 | 3.43 | C518 - left |
| pFAR4-CMVp-eGFP | 35 (40 set) | 120 | 3.43 | C518 - right |
| pFAR4-CMVp-BDNF-NT3 | 34 (40 set) | 120 | 3.53 | C516 - left |
| pFAR4-CMVp-eGFP | 36 (40 set) | 120 | 3.33 | C516 - right |
| pFAR4-CMVp-eGFP | 40 (40 set) | 95 | 2.38 | C517 - left |
| pFAR4-CMVp-BDNF-NT3 | 28 (40 set) | 120 | 4.29 | C517 - right |
| | Avg current 34.1 ± 1.6 mA | 117.5 ± 2.5 V Average Voltage achieved across groups | 3.55 ± 0.24 kΩ (n = 10) Average ± s.e.m resistance across groups | |

**Table S3. Pulse parameters and brain resistivity for *in vivo* DNA electrotransfer in guinea pig brain using the clinical CC-GET device**

| **Plasmid (DNA 2 µg/µl in 10% sucrose carrier)** | | **mean pulse amplitude (mA)** | **mean applied voltage (V)** | **Local resistance (kΩ)** | **Pulse profile (number x duration)** | **Animal ID** |
|---|---|---|---|---|---|---|
| pMK-CAGp-eGFP | | 10 | 40 | 4 | 3 x 100 ms | GP457 |
| pAd-CMVp-hrGFP* | | 10 | 25 | 2.5 | 3 x 100 ms | GP452 |
| pFAR4-CMVp-eGFP | | 50 | 90 | 1.8 | 10 x 100 µs | GP240 |
| pFAR4-CMVp-eGFP | | 50 | 90 | 1.8 | 10 x 100 µs | GP239 |
| pJL-hSYNp-ReaChR-tdTomato + pAG-CMVp-GCaMP | | 50 | - | - | 10 x 100 µs | GP232 |
| pJL-hSYNp-ReaChR-tdTomato | | 25 | 70 | 2.8 | 10 x 100 µs | GP231 |
| pJL-hSYNp-ReaChR-tdTomato | | 25 | 60 | 2.4 | 10 x 100 µs | GP230 |
| pJL-hSYNp-ReaChR-tdTomato | | 10 | 35 | 3.5 | 10 x 100 µs | GP229 |
| pJL-hSYNp-ReaChR-tdTomato | | 50 | 90 | 1.8 | 10 x 100 µs | GP228 |
| | | **Range** | **Range** | **Average** | | |
| | | 10-50 mA | 25-90 V | 2.58 ± 0.29 kΩ | | |

* = 6.5% glucose

## Primary figure commentary (Figures 1, 2, 4, 6 and 7)

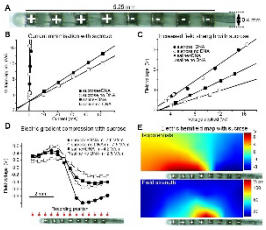

**Figure 1. Non-conductive sucrose carrier amplifies bionic array electric field strength.**
This figure demonstrates the effect of substituting a standard saline (0.9% NaCl) – based carrier for plasmid DNA GET, with isotonic 10% sucrose. (**A**) 8-electrode GET array depicting four ganged anodes (+) and cathodes (-), where this longitudinal extension of the electrode poles contributes to the electric field 'lensing'. Each of the full ring Pt/Ir electrodes is 350 µm in width, 400 µm diameter, with 350 µm spacing. (**B**) Using a current-controlled stimulator, the voltage applied to the electrodes approaches the maximum driving voltage of the stimulator with minimal current when sucrose is the carrier. Addition of DNA (sheared salmon sperm DNA, average size 2 kb, 2 µg/µl) to the normal saline carrier (0.9% NaCl) reduces conductivity, so that the voltage applied ($V_a$) to the electrode increases, which benefits GET, however, there is no appreciable additional effect of the DNA within sucrose carrier. (**C**) Measured at a single point relative to the array (e7, 0.5 mm), the rate that the sampled field voltage ($V_f$) increases with increasing $V_a$ is enhanced for DNA + saline, compared with saline alone (augmenting the advantage for GET at the level $V_a$ shown in (B)); note however, that conductivity clamping with sucrose produces a further augmentation of the $V_f$, for a given $V_a$. (**D**) Extending from the point measurement of $V_f$ in (C), here $V_f$ is measured along the length of the array, 0.5 mm lateral. The greatest change in Vf with distance (maximum electric field strength; $\Delta V_f/\Delta d$) occurs across the null point ($V_f = 0$ V) at the transition between the anode and cathode poles. This highlights the point that the absolute voltage (in the field) is irrelevant, and this close-field electric 'lensing' effect provides compression of the electric field not achievable with conventional GET electrode configurations due to current spread. (**E**) The isopotential map (hemifield; upper graphic) represents extended sampling of $V_f$ within the region around the electrode array with sucrose carrier, enabling derivation of the (2D) electric field map (at $V_a = 40$ V, lower graphic), which is circular and equivalent to suprathreshold GET field strengths for several mm orthogonal to the array.

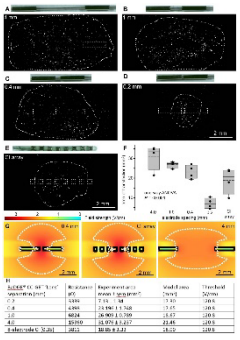

**Figure 2. Electric field 'lensing' via the CC-GET array enables spatial focusing of gene expression.**
Control of gene expression with fixed charge transfer using electric field 'lensing', via change in separation between linear extended electrode elements was used to model GET electric field threshold. Montecarlo modelling established the electric field threshold for DNA electrotransfer, utilizing data from GFP reporter expression (threshold biomarker) in HEK293 cell monolayers. The effect of separation of the CC-GET 'electro-lens' was evaluated using a modified GET array where the four ganged electrodes for one pole of the multi-electrode array were substituted for a single longitudinally extended Pt/Ir electrode of 2 mm length x 400 µm diameter, with variation of the separation with the other electrode surface, on a silicone backbone (shown in insets). CC-GET was performed using a GFP reporter plasmid including a nuclear localization signal to discretely resolve HEK293 cells expressing the transgene construct. To optimally model 'real world' intracochlear delivery we used a modified 'conductivity clamping' carrier solution comprising 9% sucrose and 0.09% saline (pH 7.4, 0.5 mM NaOH), with 2 µg/µl pAd-CMVp-hrGFPnls plasmid DNA (~ 12 µS.cm$^{-1}$ conductivity). The size of the transfected field of HEK293 cells was assessed using a fixed suprathreshold pulse train (10 x 100 µs, 400 µs interpulse interval, 30 mA square wave pulses; requiring 120 V applied; ~ 30 µC charge transfer; ~ 4 kΩ local resistance). For this fixed charge transfer, the area of transfected GFP+ve cells was found to be scalable by a factor of 4.4, from 7.13 ± 1.34 mm$^2$ to 31.08 ± 3.24 mm$^2$, when the anode - cathode separation was varied between 0.2 mm and 4 mm respectively (**A-D, F**). ANOVA indicated the significant effect on gene expression of increasing the separation between the electrodes ($P$ = 0.001).The use of two elongated electrode surfaces was found to accurately model the cochlear implant-style multi-electrode array, where the 0.4 mm separation resulted in an average area of GFP expressing cells of 23.20 ± 3.50 mm$^2$ ; not significantly different from that achieved using the reference 8 electrode GET array with equivalent separation between the gangs of four anodes and four cathodes (18.85 ± 3.33 mm$^2$, $P$ = 0.500 ANOVA, **E, F**). (**F**) Boxplots of areas of transfected cells relative to electrode separation show 25% and 75% boundaries, with 95% limits as bars; lines indicate median, dashed lines indicate means, data overlaid (n = 4 per group). (**G**) Montecarlo modelling of electric fields across the configurations (*see Supporting Information – Materials and Methods*). The dashed perimeter, established by comparison with the perimeter of the field of transfected HEK293 cells reflects the electric field threshold for DNA electrotransfer ($\Delta V_f/\Delta d$ = 120.8 ± 20.2 V/cm; mean ± SD.). (**H**) The predicted electric field threshold (120.8 V/cm) was validated *in silico* by further simulations using the clinical CC-GET array. The long-axis of the fluid ellipse around the electrodes defining the meniscus and the voltage loss across the bilayer were set as the mean of the n = 10 random values generated in (G), 0.861 mm and 14.6 V respectively. Volume of solution was 26 µl. The media electrical conductivity was taken as the average of values estimated in (G), 0.437 S/m. Supply voltage was 120 V. The data summarizes the validation simulations that accurately predicted the surface area of the field of cells with GFP reporter expression (suprathreshold GET electric field strength) using the different 'lens' separations (spacing between the opposing conductive surfaces). Images (A-D) modified from Patent ref. [9]

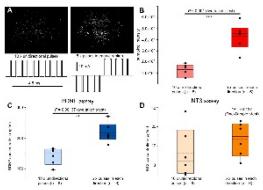

**Figure 4. Validation of recombinant BDNF and NT3 protein synthesis in HEK293 cells using the clinical CC-GET device to deliver pFAR4-CMVp-BDNF-NT3 miniplasmid and pBs-CMVp-mCHERRYnls reporter DNA**. The plasmid DNAs were delivered as a 30 µl cocktail (1 µg/µl each) in 9% sucrose + 0.09% NaCl + 0.5 mM NaOH carrier, and CC-GET performed using an 8 node electrotransfer array in tandem configuration. (**A** and **B**) Either 10 x 100 µs x 20 mA (400 µs interpulse interval) positive pulses, or 5 positive then 5 negative pulses, were utilized for CC-GET. Switching of electrode polarity within the pulse train provided a significant increase in mCherry reporter fluorescence, as well as increases in BDNF, (**C**) and NT3 (**D**) synthesis. This improved expression achieved by changing polarity may be attributable to the bias of DNA electrotransfer to the cathode-facing cell surface saturating binding efficiency. Overall, the use of alternating monophasic pulses achieved significant improvement of both BDNF and NT3 production ($P$ = 0.001; ANOVA). ELISA analysis methodology is described in Supporting Information – Materials and Methods. Data reflected in Figure 12 Patent ref.. [9] Cells were imaged and supernatant collected at 4 days post CC-GET.

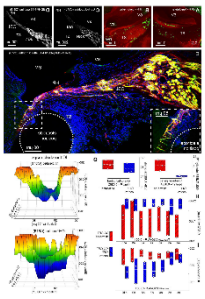

**Figure 6. Clinical CC-GET neurotrophin gene augmentation with chronic cochlear implant stimulation achieves long-term rescue of regenerated spiral ganglion neurites and reset of central auditory tuning in the cat inferior colliculus.**

(**A** and **B**) Localization of pFAR4-CMVp-eGFP expression in the lower turn of scala tympani (ST) is matched to the prior modelling of the clinical CC-GET device electric field profile (*in vivo* study of normal hearing cat, 72 hours post - CC-GET). Low magnification complementary images of hemi-sectioned cochlea (A) lateral aspect facing spiral ligament of otic capsule, (B) central modiolar wall show clusters of GFP reporter fluorescence positive mesenchymal cells in a cochlear preparation following decalcification (background autofluorescence in the red channel resolves structure). Note the absence of the GFP signal in the more apical ST region in (B), indicating the dependency of expression on the focused electric field generated by the CC-GET device. When this plasmid DNA is replaced with the therapeutic neurotrophin-encoding DNA (pFAR4-CMVp-BNDF-NT3), these cells secrete BDNF and NT3, establishing a guidance cue for directed regrowth of the spiral ganglion neurites. (**C** to **E**) regeneration of the spiral ganglion peripheral neurites is retained at the six-month endpoint in deafened cats. The majority of the regenerated fibers extend out though the osseous spiral lamina (OSL) to the normal insertion point to the sensory epithelium (habenula perforate, HP), and continue laterally beyond the insertion point of the basilar membrane with the spiral ligament, with progressive dissipation of the fiber fascicle as individual branches project through the mesenchymal cell layer in close juxtaposition to the cochlear implant electrode array. The cochlear implant array was inserted immediately after withdrawal of the clinical CC-GET device, and actively stimulated the spiral ganglion neurons to support hearing for 8 hours per day for the duration of the study. (C) control cochlea (pFAR4-CMVp-eGFP DNA delivery) TUBB3 (β3-Tubulin) immunolabelling shows scarcity of auditory nerve fibers in the osseous spiral lamina compared with the pFAR4-CMVp-BNDF-NT3 DNA - treated cochlea from the same animal, shown in (D). (E) double immunolabeling for TUBB3 and neurofilament 200, with DAPI fluorescence for nuclear labelling in a different deafened cat following neurotrophin DNA treatment. RW, round window membrane, the insertion point for the CC-GET device and then the cochlear implant array; SV, scala vestibuli; SM, scala media. Due to the restricted geometry of ST above the basal region of the cat cochlea, only the eight ganged half-band electrodes in the tip (zone 1) of the clinical CC-GET device were used for electrotransfer (10 x 100 µs x 50 mA pulses delivered at 2 kHz using a constant current controller; compliance limited to an average of 34 mA). Either the control pFAR4-CMVp-eGFP plasmid DNA, or the therapeutic pFAR4-CMVp-BDNF-NT3 plasmid DNA (2 µg/µl in 10% sucrose carrier, with 0.5 mM NaOH) was delivered into the cochlear ST through the tip of the clinical CC-GET device (50 µl at 10 µl / min), immediately prior to the electrotransfer current pulses. (**F**) Somata from cryosections (symbols distinguish average data from the three cats). (**G**) inferior colliculus auditory threshold maps from a deafened cat receiving neurotrophin-encoding DNA via CC-GET into one cochlea and eGFP–encoding DNA into the opposite cochlea, followed by continuous use of bilateral cochlear implant devices. The data reflect threshold auditory- evoked potentials recorded from 32 electrodes spanning the depth of the inferior colliculus (IC) elicited by bipolar stimulation of the respective cochlear implant arrays (electrodes 4 – 10). Stimulation of the cochlear implant array within the neurotrophin gene augmentation – treated cochlea exhibited enhanced spatial tuning at the IC array compared with that driven by stimulation of the opposite (control) cochlea. (**H**) IC spatial tuning curve (STC) width is significantly sharper as a result of the cochlear neurotrophin-gene augmentation treatment. The effect on spatial tuning curve width is most

pronounced with stimulation of cochlear implant electrode positions e6 – e9, which closely corresponds to the peak of the CC-GET electric field. The boxplot indicates 25% - 75% limits and the different symbols reflect the average for each cat (solid black line is the median, white dashed line is the mean). (**I**) Boxplots of average stimulus thresholds across all 32 IC electrodes for bipolar stimulation at each of the 7 cochlear implant electrodes, for three cats, with neurotrophin treatment in one cochlea and eGFP -encoding DNA treatment in the opposite cochlea. The data show that the cochlear neurotrophin gene augmentation treatment results in an overall reduction in excitability, which is associated with sharpening of spatial tuning.

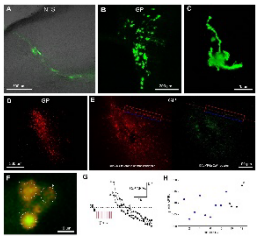

**Fig. 7. CC-GET gene delivery to guinea pig brain achieves targeted optogenetic neuromodulation.** Enablement of naked plasmid DNA electrotransfer to the brain via close-field conductance-clamping using sucrose carrier. (**A**) GFP-positive neurons in the nucleus of the tractus solitarius (NTS) region of the brainstem identified by confocal fluorescence imaging in a 50 µm cryosection taken 3 days after *in vivo* CC-GET (pFAR4-CMVp-eGFP plasmid; 10 x 100 µs x 50 mA). (**B**) Detail of eGFP-positive globus pallidus (GP) neurons imaged 7 days post CC-GET (pMK-CAGp-eGFP; 3 x 100 ms x 10 mA pulses requiring ~35V applied voltage; 50 µm cryosection). (**C**) Detail of a transfected GP neuron from the same experimental animal providing the data shown in (B). (**D**) A field of dual-plasmid transduced neurons within GP (pAG-CMVp-GCaMP5g + pJL-hSYNp-ReaChR-tdTomato; 10 x 100 µs x 50 mA; tdTomato-tagged ReaChR channel rhodopsin expression shown (300 µm vibratome section imaged via LSM as an image stack at 4 µm z resolution (95 µm total depth, 3D projection). (**E**) Detail of dual expression of ReaChR channel rhodopsin (red channel) and GCaMP5g $Ca^{2+}$ reporter (green channel) from the same animal as experimental data shown in (D). Boxed insets highlight neurons co-expressing ReaChR and GCaMP5g. (**F**) Detail of regions of interest delineating three neurons co-expressing ReaChR and GCaMP5g, where the ReaChR ion channels were photo-activated. (**G**) Intracellular $Ca^{2+}$ responses to 561 nm pulsed laser activation of the three neurons shown in (F) measured via the GCaMP5g green fluorescence emission (488 nm excitation). (**H**) Peak GCaMP5g $Ca^{2+}$ fluorescence responses for 12 neurons with photo-activation of the co-expressed ReaChR channel rhodopsin. Images from (B) and (C) are from patent ref. [8]

References

[1] G. D. Housley, C. J. Browne, E. N. Crawford, M. Klugmann, N. H. Lovell, and J. L. Pinyon, "Cochlear Implant Close-Field Electroporation," in *Handbook of Electroporation*, D. Miklavčič, Ed.: Springer, 2016, pp. 1-20.

[2] C. J. Browne *et al.*, "Mapping of bionic array electric field focusing in plasmid DNA-based gene electrotransfer," *Gene Ther,* vol. 23, no. 4, pp. 369-79, Apr 2016.

[3] J. L. Pinyon, M. Klugmann, N. H. Lovell, and G. D. Housley, "Dual-Plasmid Bionic Array-Directed Gene Electrotransfer in HEK293 Cells and Cochlear Mesenchymal Cells Probes Transgene Expression and Cell Fate," *Hum Gene Ther,* vol. 30, no. 2, pp. 211-224, Feb 2019.

[4] R. K. Shepherd *et al.*, "Platinum dissolution and tissue response following long-term electrical stimulation at high charge densities," *J Neural Eng,* Feb 12 2021.

[5] S. S. George, A. K. Wise, M. N. Shivdasani, R. K. Shepherd, and J. B. Fallon, "Evaluation of focused multipolar stimulation for cochlear implants in acutely deafened cats," *J Neural Eng,* vol. 11, no. 6, p. 065003, Dec 2014.

[6] G. E. Truett, P. Heeger, R. L. Mynatt, A. A. Truett, J. A. Walker, and M. L. Warman, "Preparation of PCR-quality mouse genomic DNA with hot sodium hydroxide and tris (HotSHOT)," *Biotechniques,* vol. 29, no. 1, pp. 52, 54, Jul 2000.

[7] C. Marie, G. Vandermeulen, M. Quiviger, M. Richard, V. Preat, and D. Scherman, "pFARs, plasmids free of antibiotic resistance markers, display high-level transgene expression in muscle, skin and tumour cells," *J Gene Med,* vol. 12, no. 4, pp. 323-32, Apr 2010.

[8] G. D. Housley, N. H. Lovell, J. Pinyon, E. N. Crawford, and C. Browne, "Electroporation system for controlled localized therapeutics delivery. *US Patent No. US 11,213,671 B2*," 2022.

[9] G. D. Housley, J. Pinyon, N. H. Lovell, and A. A. Abed, "Method and system for controlling molecular electrotransfer," *WIPO - PCT WO 2020/118383 A1,* 2020.